DISCLAIMER

This report was prepared as an account of work sponsored by an agency of the United States Government. Neither the United States Government nor any agency thereof, nor any of their employees, makes any warranty, express or implied, or assumes any legal liability or responsibility for the accuracy, completeness, or usefulness of any information, apparatus, product, or process disclosed, or represents that its use would not infringe privately owned rights. Reference herein to any specific commercial product, process, or service by trade name, trademark, manufacturer, or otherwise does not necessarily constitute or imply its endorsement, recommendation, or favoring by the United States Government or any agency thereof. The views and opinions of authors expressed herein do not necessarily state or reflect those of the United States Government or any agency thereof. Reference herein to any social initiative (including but not limited to Diversity, Equity, and Inclusion (DEI); Community Benefits Plans (CBP); Justice 40; etc.) is made by the Author independent of any current requirement by the United States Government and does not constitute or imply endorsement, recommendation, or support by the United States Government or any agency thereof.

L3:RTM.MCH.P19.06: Neutronics UQ

Pablo Ducru[1], Abdulla Alhajri[1], Isaac Meyer[1], Vladimir Sobes[2], and Benoit Forget[1]

[1]Massachusetts Institute of Technology
[2]Oak Ridge National Laboratory

September 30th, 2019

1 Introduction

This report summarizes some of the work performed in the last year on the nuclear data uncertainty tasks using the multipole representation. This approach was proposed to provide a simple and integrated way of evaluating the nuclear data uncertainty in a Monte Carlo simulation and evaluating their impact on multigroup cross sections.

As previously described, the windowed multipole format allows for a resonance based representation of the cross sections with direct Doppler broadening. This representation also lends itself nicely to the evaluation of sensitivities of resonance parameters and the direct perturbation of resonance parameters in the simulation environment. Both of these approaches rely on the need of conversion of the covariance data (File 32 of the ENDF library) into a pole and residues form: i.e. into a *multipole covariance*. Section 5 details the current pathways that have been used so far to achieve this.

In order to verify the conversion process of the covariance data, the sensitivies to the resonance parameters and the sampling from these parameters, an analytical benchmark of the slowing process was developed. The benchmark provides a closed-form solution for the flux in the presence of Hydrogen and multiple resonant nuclides. Section 2 details the analytical benchmark and provides the closed-form solutions for the flux and its sensitivity to resonance parameters. A verification of the proposed methodology is performed and compared with the analytic solution to demonstrate the accuracy of the benchmark and the applicability of our embedded resonance perturbation approach in a small Monte Carlo code. Papers are currently being drafted documenting the benchmark and the generation of sensitivities.

As paths to best generate multipole covariance matrices are being compared, we also explored new methods to propagate nuclear data uncertainty across the Monte Carlo neutron transport calculation. Section 4 studies the use of multipole covariance matrices to perform sensitivity analysis. Section 3.2 documents the results of our investigations into a new way of propagating nuclear data uncertainty across Monte Carlo transport simulations by sampling new epistemic cross sections for each new neutron.

2 Analytic Benchmark: a reference solution for uncertainty propagation

The purpose of this section is to describe the efforts made to establish a reference solution to verify and validate the results of the new uncertainty propagation methods being developed at MIT, using the pole representation formalism.

We have derived an analytic benchmark for the neutron slowing down problem, thereby solving the flux and its sensitivities in closed-form solution. These results are the subject of an article being submitted to the *Computer Physics Communications* journal [1].

2.1 Key results from the analytic benchmark

We here synthesize the novel results derived for our analytic benchmark under the hypotheses listed in section 2.1.1.

2.1.1 Benchmark hypotheses

A few simplifications were needed in order to make the solution of the slowing down problem analytical:

- time-independent cross sections,
- infinite homogeneous medium,
- no external source $Q(E) = 0$,
- piece-wise flat fission spectrum $\chi(E) \coloneqq \chi_0 \mathbb{1}\left[E < E_\infty\right]$, where $E_\infty \in \mathbb{R}_+$ is a cutoff energy,
- isotropic scattering in the center on mass, from an atomic weight ratio of one (Hydrogen, no Plazeck transients),
- cross sections $\sigma(E)$ are rational fractions in $\sqrt{E}$, which is always verified for neutral particles without threshold in the case of semi-classical R-matrix theory.

These hypotheses simplify the transport equation to a purely down-scattering problem in energy:

$$\Sigma_t(E)\psi_k(E) - \int_E^{E_\infty} \mathrm{d}E' \frac{\Sigma_s(E')}{E'}\psi_k(E') = \frac{\chi(E)}{k}\int_0^{E_\infty} \mathrm{d}E' \nu\Sigma_f(E')\psi_k(E') \tag{1}$$

2.1.2 Generic Reference Solutions

The following explicit analytic solutions were established:

$$\Sigma_t(E)\psi_k(E) = \left[\ \Sigma_t\psi_\alpha\big|_{E_0}\ \right] \mathrm{e}^{-\int_0^E \mathsf{D_S}(E')\mathrm{d}E'} \mathbb{1}\Big[E \in [E_0, E_\infty]\Big] \tag{2}$$

where the here defined *down-scattering ratio* plays a central role

$$\mathsf{D_S}(E) \coloneqq \frac{\Sigma_s(E)}{E\Sigma_t(E)} \tag{3}$$

Once the flux has been obtained by equation (2), the associated eigenvalue k is obtained by any of the following equations:

$$k = \chi_0 \int_0^{E_\infty} \mathrm{d}E' \frac{\nu\Sigma_f(E')}{\Sigma_t(E')} \mathrm{e}^{\int_{E'}^{E_\infty} \mathsf{D_S}(E')\mathrm{d}E'} \tag{4}$$

$$k = \frac{\chi_0 \int_0^{E_\infty} \nu\Sigma_f(E')\psi_k(E')\mathrm{d}E'}{\Sigma_t(E_\infty)\psi_k(E_\infty)} \tag{5}$$

$$k = \frac{\int_0^{E_\infty} \nu\Sigma_f(E')\psi_k(E')\mathrm{d}E'}{\int_0^{E_\infty} \left[\Sigma_t(E)\psi_k(E) - \int_E^{E_\infty} \mathrm{d}E' \frac{\Sigma_s(E')}{E'}\psi_k(E')\right]\mathrm{d}E} \tag{6}$$

2.1.3 Explicit Reference Solutions

Remarkably, we were able to take these generic results of the flux (2) and k-eigenvalue (4) one step further, and provide explicit, closed-form solutions.

First, the change of variable $x = \sqrt{E}$ is performed,

$$\mathsf{D_S}^\alpha(x)\mathrm{d}x \ \coloneqq \mathsf{D_S}^\alpha(E)\mathrm{d}E \tag{7}$$

Importantly, the Jacobian of the transformation is included in the definition of the down-scattering ratio, which here behaves like a flux.

Then, we perform the partial fraction decomposition of the scattering ratio in the $\sqrt{E}$ space:

$$\mathsf{D_S}^\alpha(x) \ = \sum_{n=1}^{N_p} \frac{a_n}{x - b_n} \tag{8}$$

where $\{a_n\}$ and $\{b_n\}$ are complex conjugate poles and residues, entailing $\mathsf{D_S}^{\alpha}(x)$ is real for real x. Let us here note that performing the latter partial fraction decomposition is a difficult problem, for which we have developed specific methods that are the object of a forthcoming publication.

A careful study of the number of poles and residues of the $\mathsf{D_S}$ factor shows that on the principal sheet of the Riemann surface generated by the mapping $E \longleftrightarrow \sqrt{E}$, the number of poles stemming from the R-matrix formalism of nuclear reactions cross sections is exactly:

$$N_p \coloneqq 2(2N_\lambda + \sum_c \ell_c) + 1 \tag{9}$$

More importantly, the $\mathsf{D_S}$ factor is always a simple rational fraction, without principle polynomial terms. In line with some of our recent work, the $\mathsf{D_S}(x)$ ratio could be approximated with rational fractions using the vector fitting algorithm [2].

By injecting it in our derived generic form of the flux (2), the rational fraction expansion (8) of the $\mathsf{D_S}(x)$ ratio yields the following closed-form flux solution:

$$\psi(E) = \psi_0 \frac{\left[\Sigma_t + \alpha\sqrt{\frac{m_{\text{ne.}}}{2E}}\right]_{E_0=0}}{\left[\Sigma_t + \alpha\sqrt{\frac{m_{\text{ne.}}}{2E}}\right]_{E=E}} \prod_{n=1}^{N_p} \left(\frac{\sqrt{E_0} - b_n}{\sqrt{E} - b_n}\right)^{a_n} \tag{10}$$

2.1.4 Verification

To verify our analytic solutions, we compared them to an analog Monte-Carlo code using the same hypothesis. A benchmark problem was created from the first resonance of Pu-239, the two first resonances of Hf-177 and hydrogen. The resulting macroscopic cross sections are reported in Figure 1 and Figure 2.

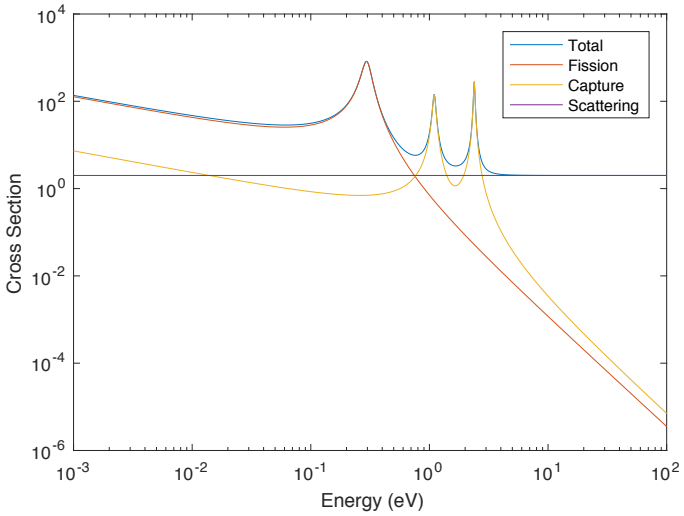

Figure 1: Macroscopic cross sections for the analytic benchmark: the first fission resonance of Pu-239, the two first capture resonances of Hf-177, and flat isotropic hydrogen moderation. Comparing the Analytic code and the Monte-Carlo code.

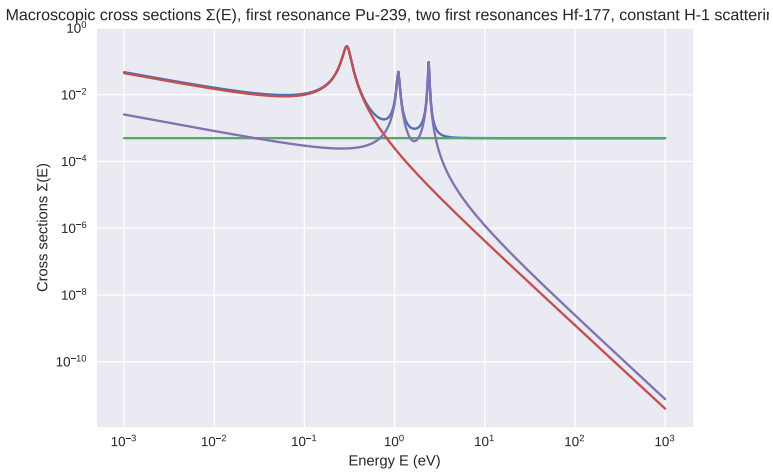

Figure 2: Macroscopic cross sections for the analytic benchmark: the first resonance of Pu-239, the two first resonances of Hf-177, and flat isotropic hydrogen moderation. Comparing the Analytic code and the Monte-Carlo code.

The associated flux was computed for both the Monte-Carlo calculation, and the analytic solution (10), and recorded in Figure 3 and Figure 4,

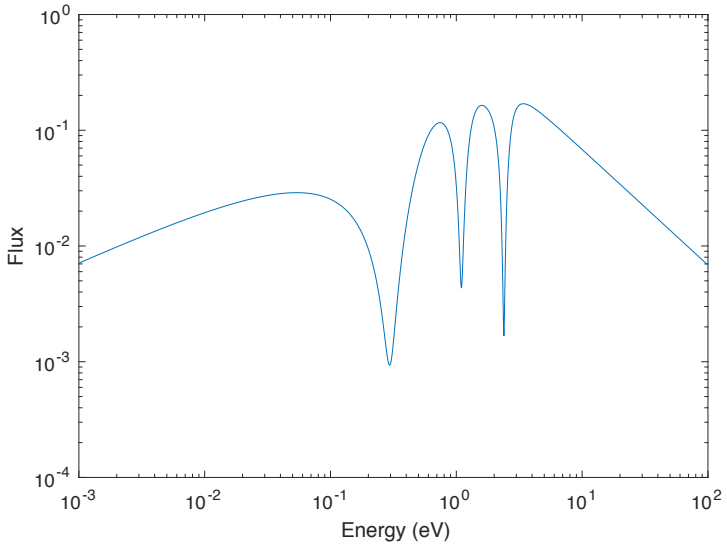

Figure 3: Flux amplitude $\psi(E)$ obtained from the analytic equation (10), on the macroscopic cross sections from Figure 1

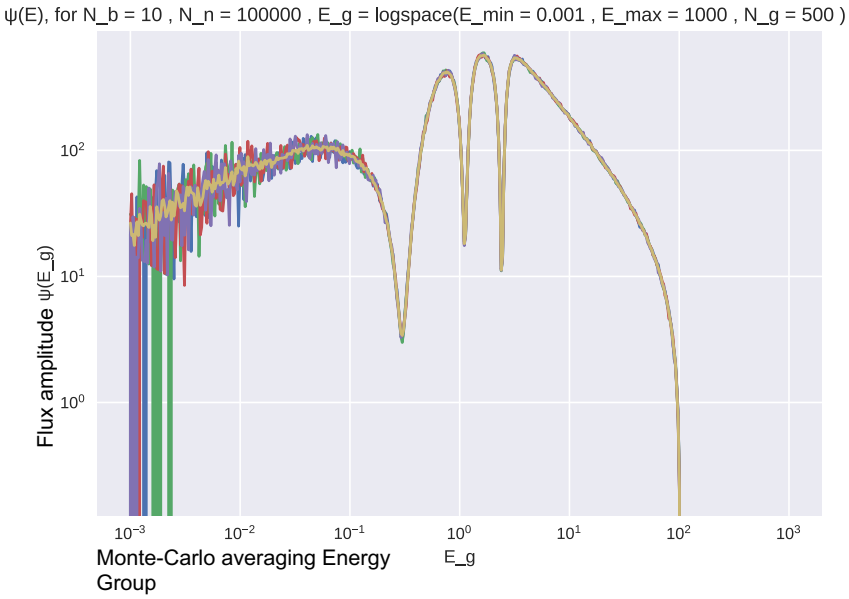

Figure 4: Flux amplitude $\psi(E)$ obtained from Monte Carlo code to validate the results of the analytic benchmark, on the macroscopic cross sections from Figure 2. We ran 1,000,000 neutrons in 10 batches of 100,000.

In addition to the analog Monte Carlo code, a set of ENDF files describing the isotopes in the analytic benchmark were created. The ENDF files were converted into OpenMC HDF5 cross section files, and the analytic benchmark problem was run in OpenMC. This will allow us to test the sensitivity obtained via the multipole sensitivity capability in OpenMC to be validated against an analytic solution.

The histogram of the batch estimates of the associated k-eigenvalue is recorded in Figure 5.

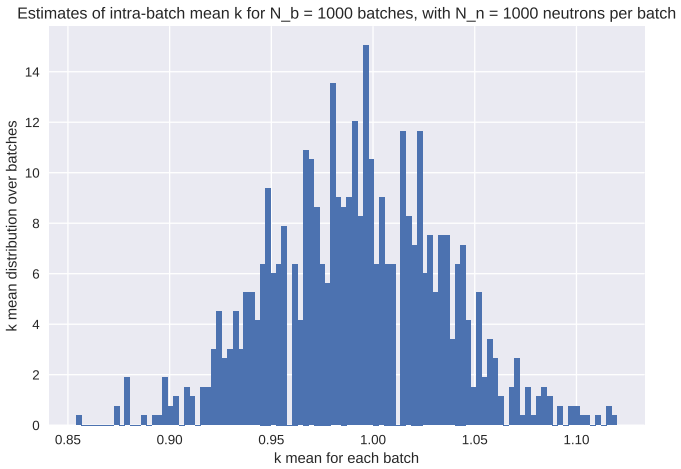

Figure 5: Aleatoric batch distributions of k, for problem in Figure 2, for each batch of 1000 neutrons, the mean k_batch is computed and recorded in the histogram. We ran 1,000,000 neutrons in 1000 batches of 1000.

These compare to the analytically computed solution of:

$$k_{\text{analytic}} = 0.990932 \tag{11}$$

The analytic benchmark will prove useful in validating the uncertainty propagation methods being proposed, but could also be particularly useful for validating slowing down solvers and multigroup structures in the generation of self-shielded coarse group libraries.

2.2 Analytic sensitivities for the flux and k-eigenvalue

Taking this analytical solution further, allows us to derive analytic results for the sensitivities of the flux and the associated k-eigenvalue with respect to an infinitesimal change in any given resonance parameter or cross section.

2.2.1 Deriving generic analytic sensitivities

The cross sections are functions of the incoming neutron kinetic energy E, and are parametrized by resonance parameters, which we shall generically write Γ. This makes them mathematically a function of both E and Γ. For clarity, we shall not write the Γ dependence explicitly. Functional differentiation allows us to express the sensitivity of the flux amplitude to a change in a generic resonance parameter Γ as:

$$\frac{\partial\psi(E)}{\partial\Gamma} = \int_0^{E_\infty} \left[\frac{\partial\Sigma_i(E')}{\partial\Gamma}\right] \left[\frac{\partial\psi(E)}{\partial\Sigma_i(E')}\right] \mathrm{d}E' \tag{12}$$

where we recall that $\Sigma_t^\alpha(E) \coloneqq \Sigma_t(E) + \alpha\sqrt{\frac{m_{\text{ne.}}}{2E}} \coloneqq \Sigma_s(E) + \Sigma_\gamma(E) + \Sigma_f(E) + \alpha\sqrt{\frac{m_{\text{ne.}}}{2E}} \coloneqq \Sigma_s + \Sigma_a^\alpha(E)$, and $i = \{s\,,\ a\}$ indicates the sensitivity to either the absorption $\Sigma_a^\alpha(E)$ or the constant scattering $\Sigma_{s,0}$ cross section.

We can then perform functional differentiation as follows:

$$\frac{\partial\psi(E)}{\partial\Sigma_i(E')} = \psi_0\Sigma_t^\alpha(0)\left[\mathrm{e}^{-\int_0^E \frac{\Sigma_s(y)}{y\Sigma_t^\alpha(y)}\mathrm{d}y} \frac{\partial}{\partial\Sigma_i(E')}\left(\frac{1}{\Sigma_t^\alpha(E)}\right) + \frac{1}{\Sigma_t^\alpha(E)}\frac{\partial}{\partial\Sigma_i(E')}\left(\mathrm{e}^{-\int_0^E \frac{\Sigma_s(y)}{y\Sigma_t^\alpha(y)}\mathrm{d}y}\right)\right] \tag{13}$$

we then express this functional differentiation using the Dirac δ distribution and its integration to a Heaviside function:

$$\frac{\partial\psi(E)}{\partial\Sigma_i(E')} + \psi(E)\left[\frac{1}{\Sigma_t^\alpha(E')}\delta(E-E') + \mathbb{1}\left[E' \le E\right]\frac{\partial}{\partial\Sigma_i(E')}\left(\frac{\Sigma_s(E')}{E'\Sigma_t^\alpha(E')}\right)\right] = 0 \tag{14}$$

or, exhibiting the central role of the down-scattering ratio $\mathsf{D_S}(E)$,

$$\frac{\partial\psi(E)}{\partial\Sigma_i(E')} = -\psi(E)\left[\frac{1}{\Sigma_t^\alpha(E')}\delta(E-E') + \mathbb{1}\left[E' \le E\right]\frac{\partial}{\partial\Sigma_i(E')}\left(\frac{\Sigma_s(E')}{E'\Sigma_t^\alpha(E')}\right)\right] \tag{15}$$

Recognizing the derivative of the $\mathsf{D_S}(E')$ ratio, $\frac{\partial}{\partial\Sigma_i(E')}\left(\frac{\Sigma_s(E')}{E'\Sigma_t^\alpha(E')}\right) = \frac{\partial\mathsf{D_S}(E')}{\partial\Sigma_i(E')}$, this partial differential equation (15) on the sensitivities of the flux amplitudes to a small change in cross section can then be integrated in (12), using the chain rule $\frac{\partial\Sigma_i(E')}{\partial\Gamma}\frac{\partial}{\partial\Sigma_i(E')} = \frac{\partial}{\partial\Gamma}$ to yield the sensitivity to resonance parameters:

$$\frac{\partial\psi(E)}{\partial\Gamma} + \psi(E)\left[\frac{1}{\Sigma_t^\alpha(E)}\left(\frac{\partial\Sigma_i(E)}{\partial\Gamma}\right) + \int_0^E \frac{\partial\mathsf{D_S}}{\partial\Gamma}(E')\mathrm{d}E'\right] = 0 \tag{16}$$

This is the generic, integral solution for the flux sensitivity to a change of resonance parameter, Γ.

Using the flux sensitivity (16), we can now establish the associated eigenvalue sensitivities, by taking the partial derivatives:

$$\frac{\partial k_\infty}{\partial\Sigma_i(E')} = \frac{\nu\int_0^{E_0} dE\left[\psi(E)\frac{\partial\Sigma_f(E)}{\partial\Sigma_i(E')} + \Sigma_f(E)\frac{\partial\psi(E)}{\partial\Sigma_i(E')}\right] - k_\infty\left[\psi(E_\infty)\frac{\partial\Sigma_t^\alpha(E_\infty)}{\partial\Sigma_i(E')} + \Sigma_t^\alpha(E_\infty)\frac{\partial\psi(E_\infty)}{\partial\Sigma_i(E')}\right]}{\Sigma_t^\alpha(E_\infty)\psi(E_\infty)} \tag{17}$$

yielding

$$\frac{\partial k_\infty}{\partial\Sigma_i(E')} = \frac{\nu\left[\delta_{i=f} - \frac{\Sigma_f(E')}{\Sigma_t^\alpha(E')}\right]\psi(E') - \left[\nu\int_0^{E'} dE\Sigma_f(E)\psi(E) + k_\infty\mathbb{1}\left[E' \le E_\infty\right]\right]\frac{\partial}{\partial\Sigma_i(E')}\left(\frac{\Sigma_s(E')}{E'\Sigma_t^\alpha(E')}\right)}{\Sigma_t^\alpha(E_\infty)\psi(E_\infty)} \tag{18}$$

These novel results enable us to establish a benchmark for the group collapsing and group-wise sensitivities of the k-eigenvalue.

Moreover, the functional integration can be performed to obtain the sensitivity to a given resonance parameter, yielding:

$$\frac{\partial k_\infty}{\partial \Gamma} = \frac{\nu \int_0^{E_0} dE \left[\psi(E)\frac{\partial \Sigma_f(E)}{\partial \Gamma} + \Sigma_f(E)\frac{\partial \psi(E)}{\partial \Gamma}\right] - k_\infty \int_0^{E_0} dE \left[\psi(E)\frac{\partial \Sigma_a(E)}{\partial \Gamma} + \Sigma_a(E)\frac{\partial \psi(E)}{\partial \Gamma}\right]}{\int_0^{E_0} dE \Sigma_a(E)\psi(E)} \tag{19}$$

where the flux derivatives with respect to the resonance parameters are obtained through equation (16), or explicitly through (23).

2.2.2 Validation and verification

Validation and verification has been performed under the auspices of comparison with Total Monte Carlo. Here, we perturb the resonance parameters, yielding a range of possible macroscopic cross sections given the uncertainty in the resonance parameters, as depicted in Figure 6.

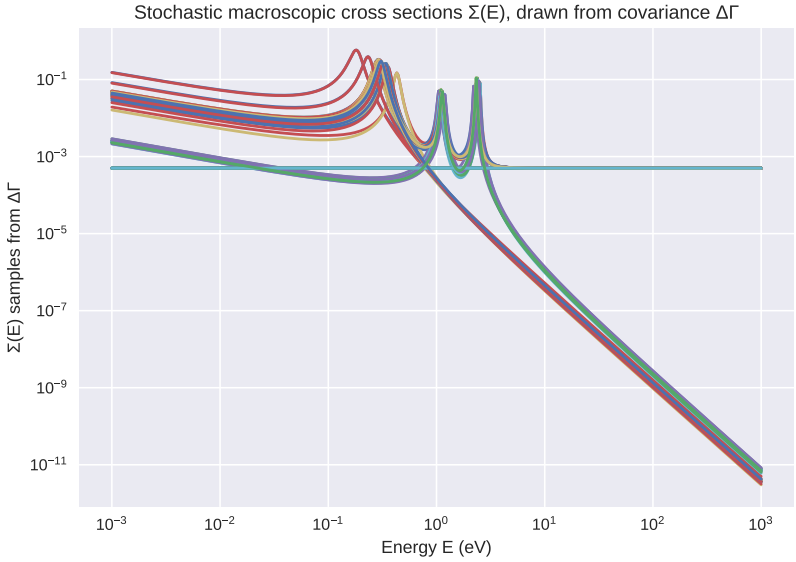

Figure 6: Stochastic macroscopic cross sections for the analytic benchmark, generated from Normal-sampling of the mean Γ and co-variance $\Delta\Gamma$ matrix of the resonance parameters.

Following the Fast-Total-Monte-Carlo method developed by D. Rochman [3], we change the cross sections at each new batch within the Monte Carlo calculation. This enables us to compute a batch $k_{\text{batch}}^{\Gamma_{\text{batch}}}$ for different Γ values, and analyze the propagated distributions. The results for both the flux and the k eigenvalue are here recorded in Figures 7 and 8, respectively.

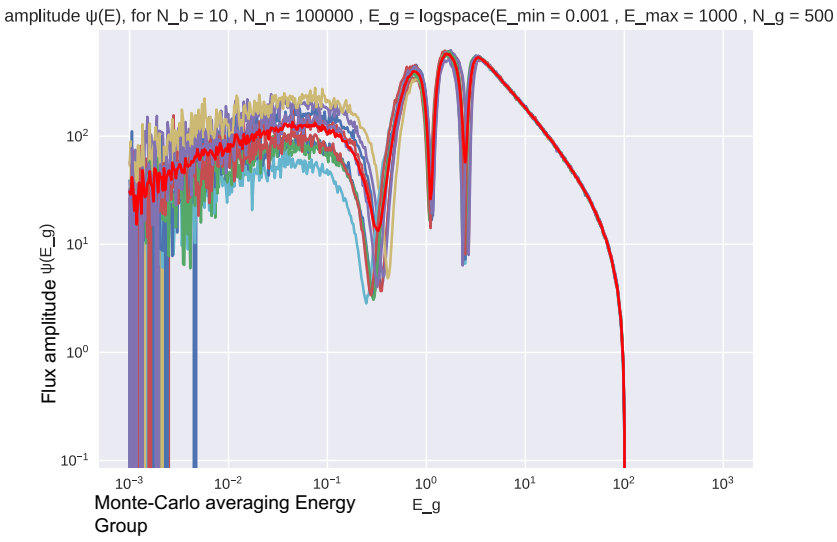

Figure 7: Batch embedded epistemic uncertainty flux amplitude $\psi(E)$ obtained from Monte Carlo code to validate the results of the analytic benchmark. We ran 1,000,000 neutrons in 10 batches of 100,000.

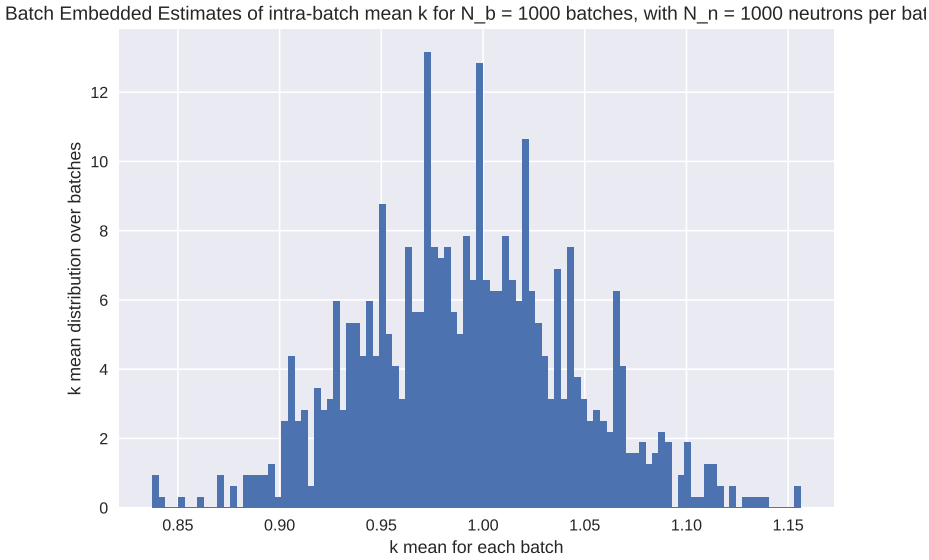

Figure 8: Aleatoric batch distributions of k. We ran 1,000,000 neutrons in 1000 batches of 1000 neutrons.

2.2.3 Deriving explicit analytic sensitivities

As for the flux and the eigenvalue, the key to deriving the explicit, closed-form analytic sensitivities lies in the partial fraction expansion of the $\mathsf{D_S}$ down-scattering ratio, the partial differential of which we now take with respect to some resonance parameter Γ.

Indeed, let us here note that equation (16) will necessitate the energy integral of the partial derivatives of the $\mathsf{D_S}$ ratio with respect to the resonance parameters $\frac{\partial \mathsf{D_S}^{\alpha}}{\partial \Gamma}$:

$$\mathcal{G}_E := \int_0^E \frac{\partial \mathsf{D_S}^{\alpha}}{\partial \Gamma}(E')\mathrm{d}E' = \int_0^{\sqrt{E}} \frac{\partial \mathsf{D_S}^{\alpha}}{\partial \Gamma}(x)\mathrm{d}x \tag{20}$$

Using the partial fraction decomposition (8) of the $\mathsf{D_S}$ ratio (3), integral (22) can be readily solved by noticing that

$$\frac{\partial \mathsf{D_S}^{\alpha}}{\partial \Gamma}(x) \;\; = \sum_{n=1}^{N_p} \frac{\frac{\partial a_n}{\partial \Gamma}}{x - b_n} + \frac{a_n \frac{\partial b_n}{\partial \Gamma}}{(x - b_n)^2} \tag{21}$$

where we observe that we now have poles of order two in $x = \sqrt{E}$ space. From partial fraction decomposition (21), it stems that (20) integrates to:

$$\mathcal{G}_E = \sum_{n=1}^{N_p} \frac{\partial a_n}{\partial \Gamma} \ln\left(\frac{\sqrt{E} - b_n}{\sqrt{E_0} - b_n}\right) + a_n \frac{\partial b_n}{\partial \Gamma}\left[\frac{1}{\sqrt{E_0} - b_n} - \frac{1}{\sqrt{E} - b_n}\right] \tag{22}$$

The same procedure as for the flux amplitude in equation (16) can now be deployed, whereby we perform a partial fraction decomposition (21) in $x = \sqrt{E}$ space of the integrand $\frac{\partial \mathsf{D_S}}{\partial \Gamma}$, from which we analytically integrate equation (16) using integral (22), we then get the following explicit logarithmic derivative of the flux with respect to some generic resonance parameter Γ:

$$\frac{1}{\psi(E)}\frac{\partial \psi(E)}{\partial \Gamma} + \left[\frac{1}{\Sigma_t^{\alpha}(E)}\frac{\partial \Sigma_i(E)}{\partial \Gamma} + \sum_{n=1}^{N_p} \frac{\partial a_n}{\partial \Gamma} \ln\left(\frac{\sqrt{E} - b_n}{\sqrt{E_0} - b_n}\right) + a_n \frac{\partial b_n}{\partial \Gamma}\left[\frac{1}{\sqrt{E_0} - b_n} - \frac{1}{\sqrt{E} - b_n}\right]\right] = 0 \tag{23}$$

Here again $E_0 = 0$, and the fact that the a_n and b_n are complex conjugates entails the argument in the complex logarithm cancels out.

This novel closed-form solution provides the sensitivities of the flux to a change in resonance parameters.

2.2.4 Deriving the Adjoint

In addition to the forward problem, the analytic benchmark was converted into an an adjoint problem. This section will demonstrate the derivation and application of the adjoint problem. The transport equation can be written in operator form in the following way

$$T\psi \equiv \Sigma_T(E)\psi(E) - \int_E^{E_\infty} \frac{\Sigma_s(E')}{E'}\psi(E')dE' - \frac{\chi(E)}{k}\int_{E_0}^{E_\infty} \nu\Sigma_f(E')\psi(E')dE' = 0 \tag{24}$$

The adjoint operator, $T^{\dagger}$, is defined such as

$$< f, Tg > = < T^{\dagger}f, g > \quad \forall f, g \in F[E, E_\infty] \to R \tag{25}$$

and the inner product is defined as

$$< f, g > = \int_{E_0}^{E_\infty} f(E)g(E)dE \tag{26}$$

We can know begin deriving the adjoint Transport operator:

$$< f, Tg > = \int_{E_0}^{E_\infty} \left[f(E)\Sigma_T(E)g(E) - f(E)\int_E^{E_\infty} \frac{\Sigma_s(E')}{E'}g(E')dE' - f(E)\frac{\chi(E)}{k}\int_{E_0}^{E_\infty} \nu\Sigma_f(E')g(E')dE'\right]dE \tag{27}$$

separating out the integrals:

$$\begin{aligned} < f, Tg > = \int_{E_0}^{E_\infty} f(E)\Sigma_T(E)g(E)dE &- \int_{E_0}^{E_\infty}\left[f(E)\int_E^{E_\infty} \frac{\Sigma_s(E')}{E'}g(E')dE'\right]dE \\ &- \int_{E_0}^{E_\infty}\left[f(E)\frac{\chi(E)}{k}\int_{E_0}^{E_\infty} \nu\Sigma_f(E')g(E')dE'\right]dE \end{aligned} \tag{28}$$

Now that the integral has been separated into three parts, we can find the adjoint of each part separately.

$$Tg = T_1 g + T_2 g + T_3 g \tag{29}$$

and

$$T_1 g = \Sigma_T(E) g(E) \tag{30}$$

$$T_2 g = -\int_E^{E_\infty} \frac{\Sigma_s(E')}{E'} g(E') dE' \tag{31}$$

$$T_3 g = -\frac{\chi(E)}{k} \int_{E_0}^{E_\infty} \nu\Sigma_f(E') g(E') dE' \tag{32}$$

It is clear that T_1 is self adjoint, or in other words $T_1 = T_1^\dagger$.
Moving on to T_2:

$$< f, T_2 g >= -\int_{E_0}^{E_\infty} \left[f(E) \int_E^{E_\infty} \frac{\Sigma_s(E')}{E'} g(E') dE' \right] dE = -\int_{E_0}^{E_\infty} \int_E^{E_\infty} f(E) \frac{\Sigma_s(E')}{E'} g(E') dE' dE \tag{33}$$

We can now change the order of integration by modifying the bounds of the integrals.

$$< f, T_2 g >= -\int_{E_0}^{E_\infty} \int_E^{E_\infty} f(E) \frac{\Sigma_s(E')}{E'} g(E') dE' dE = -\int_{E_0}^{E_\infty} \int_{E_0}^{E} f(E) \frac{\Sigma_s(E')}{E'} g(E') dE dE' \tag{34}$$

$$= -\int_{E_0}^{E_\infty} \frac{\Sigma_s(E')}{E'} g(E') \int_{E_0}^{E} f(E) dE dE' \tag{35}$$

$$\implies T_2^\dagger f = -\frac{\Sigma_s(E)}{E} \int_{E_0}^{E} f(E') dE' \tag{36}$$

Finally, we move on to T_3

$$< f, T_3 g >= -\int_{E_0}^{E_\infty} \left[f(E) \frac{\chi(E)}{k} \int_{E_0}^{E_\infty} \nu\Sigma_f(E') g(E') dE' \right] dE = -\int_{E_0}^{E_\infty} \int_{E_0}^{E_\infty} f(E) \frac{\chi(E)}{k} \nu\Sigma_f(E') g(E') dE' dE \tag{37}$$

By once again changing the order of integration, it is clear that

$$T_3^\dagger f = -\frac{\nu\Sigma_f(E)}{k} \int_{E_0}^{E_\infty} \chi(E') f(E') dE' \tag{38}$$

Using the fact that $\chi(E)$ is constant in the region between E_0 and E_∞, we can write

$$T_3^\dagger f = -\frac{\chi\nu\Sigma_f(E)}{k} \int_{E_0}^{E_\infty} f(E') dE' \tag{39}$$

Now we can put it all together and write the adjoint operator as follows:

$$T^\dagger f = \Sigma_T(E) f(E) - \frac{\Sigma_s(E)}{E} \int_{E_0}^{E} f(E') dE' - \frac{\chi\nu\Sigma_f(E)}{k} \int_{E_0}^{E_\infty} f(E') dE' \tag{40}$$

2.2.5 Deriving the adjoint flux

The adjoint flux, $\phi(E)$, is the flux that solves the adjoint equation:

$$T^{\dagger}\phi = 0 \tag{41}$$

The adjoint transport equation is expanded to this form

$$\Sigma_T(E)\phi(E) - \frac{\Sigma_s(E)}{E}\int_{E_0}^{E}\phi(E')dE' = \frac{\chi\nu\Sigma_f(E)}{k}\int_{E_0}^{E_\infty}\phi(E')dE' \tag{42}$$

We note that the eigenfunctions, $\phi(E)$ that satisfy the adjoint equation are invariant to scaling. We can therefore add the normalization constraint:

$$\int_{E_0}^{E_\infty}\phi(E')dE' = 1 \tag{43}$$

Our equation now becomes

$$\Sigma_T(E)\phi(E) - \frac{\Sigma_s(E)}{E}\int_{E_0}^{E}\phi(E')dE' = \frac{\chi\nu\Sigma_f(E)}{k} \tag{44}$$

Dividing through by $\frac{E}{\Sigma_s(E)}$:

$$\frac{E\Sigma_T(E)}{\Sigma_s(E)}\phi(E) - \int_{E_0}^{E}\phi(E')dE' = \frac{\chi\nu E\Sigma_f(E)}{k\Sigma_s(E)} \tag{45}$$

We notice that downscattering ratio appears in the equation

$$\frac{1}{D_S(E)}\phi(E) - \int_{E_0}^{E}\phi(E')dE' = \frac{\chi\nu E\Sigma_f(E)}{k\Sigma_s(E)} \tag{46}$$

We define the fission ratio, $F_S \equiv \frac{\chi\nu E\Sigma_f(E)}{k\Sigma_s(E)}$, so the equation becomes

$$\frac{1}{D_S(E)}\phi(E) - \int_{E_0}^{E}\phi(E')dE' = F_S(E) \tag{47}$$

We can take the derivative of the equation to convert it into a linear first order ordinary differential equation.

$$\phi'(E) - \left[\frac{D_S'(E)}{D_S(E)} + D_S(E)\right]\phi(E) = D_S(E)F_S'(E) \tag{48}$$

This equation can be solved with standard ODE methods using an integrating factor, the solution becomes

$$\phi(E) = e^{-\mu(E)}\left[\phi_0 + \int_{E_0}^{E} e^{\mu(E')}D_S(E')F_S'(E')dE'\right] \tag{49}$$

where the integrating factor $\mu(E)$ is defined as

$$\mu(E) = -\int_{E_0}^{E}\left[\frac{D_S'(E')}{D_S(E')} + D_S(E')\right]dE' = -\int_{E_0}^{E}\frac{D_S'(E')}{D_S(E')}dE' - \int_{E_0}^{E}D_S(E')dE' \tag{50}$$

$$\mu(E) = -\ln\frac{D_S(E)}{D_S(E_0)} - \int_{E_0}^{E}D_S(E')dE' \tag{51}$$

$$e^{\mu(E)} = \frac{D_S(E_0)}{D_S(E)}e^{-\int_{E_0}^{E}D_S(E')dE'} = \frac{D_S(E_0)}{D_S(E)}\prod\left(\frac{\sqrt{E_0}-b_n}{\sqrt{E}-b_n}\right)^{a_n} \tag{52}$$

Where we utilize the fact that $D_S(E)$ is a rational function and can be rewritten as a pole expansion $\frac{1}{E}\sum\frac{a_n}{\sqrt{E}-b_n}$

Therefore the adjoint flux becomes

$$\phi(E) = \frac{D_S(E)}{D_S(E_0)} \prod \left(\frac{\sqrt{E} - b_n}{\sqrt{E_0} - b_n} \right)^{a_n} \left[\phi_0 + \int_{E_0}^{E} D_S(E_0) \prod \left(\frac{\sqrt{E_0} - b_n}{\sqrt{E'} - b_n} \right)^{a_n} F'_S(E') dE' \right] \tag{53}$$

Where ϕ_0 is a normalization factor and can be calculated by forcing $\int_{E_0}^{E_\infty} \phi(E')dE' = 1$
This comes out to

$$\phi_0 = \frac{1 - \int_{E_0}^{E_\infty} D_S(E) \prod \left(\sqrt{E} - b_n \right)^{a_n} \left(\int_{E_0}^{E} F'_S(E') \prod \left(\sqrt{E'} - b_n \right)^{-a_n} dE' \right) dE}{\int_{E_0}^{E_\infty} \frac{D_S(E)}{D_S(E_0)} \prod \left(\frac{\sqrt{E} - b_n}{\sqrt{E_0} - b_n} \right)^{a_n} dE} \tag{54}$$

Resolving the integral in the denominator,

$$\phi_0 = \frac{1 - \int_{E_0}^{E_\infty} D_S(E) \prod \left(\sqrt{E} - b_n \right)^{a_n} \left(\int_{E_0}^{E} F'_S(E') \prod \left(\sqrt{E'} - b_n \right)^{-a_n} dE' \right) dE}{\frac{1}{D_S(E_0)} \left[\prod \left(\frac{\sqrt{E_\infty} - b_n}{\sqrt{E_0} - b_n} \right)^{a_n} - 1 \right]} \tag{55}$$

2.2.6 Eigenvalue sensitivities

Given our transport equation, it is our goal to develop a set of relations that describe the sensitivities of the eigenvalue, and the flux, to arbitrary parameters. Starting once again from the transport equation, in operator form:

$$L\psi = \lambda F \psi \tag{56}$$

Where $\lambda = 1/k$, and the operators are defined as:

$$L\psi \equiv \Sigma_T(E)\psi(E) - \int_E^{E_\infty} \frac{\Sigma_s(E')}{E'} \psi(E') dE' \tag{57}$$

and

$$F\psi \equiv \chi(E) \int_{E_0}^{E_\infty} \nu\Sigma_f(E')\psi(E')dE' \tag{58}$$

We start by taking the derivative of the transport equation with respect to an arbitrary parameter x. For purposes of notation, the superscript (n) denotes the n-th derivative with respect to x.
at first order,

$$L^{(1)}\psi + L\psi^{(1)} = \lambda^{(1)} F\psi + \lambda F^{(1)}\psi + \lambda F \psi^{(1)} \tag{59}$$

for second order, we simply take the derivative a second time,

$$L^{(2)}\psi + 2L^{(1)}\psi^{(1)} + L\psi^{(2)} = \lambda^{(2)} F\psi + \lambda F\psi^{(2)} + \lambda F^{(2)}\psi + 2\lambda^{(1)} F\psi^{(1)} + 2\lambda^{(1)} F^{(1)}\psi + 2\lambda F^{(1)}\psi^{(1)} \tag{60}$$

and the general n-th order derivative is

$$\sum_{k=0}^{n} \binom{n}{k} L^{(k)} \psi^{(n-k)} = \sum_{k=0}^{n} \sum_{j=0}^{k} \binom{n}{k} \binom{k}{j} \lambda^{(j)} F^{(k-j)} \psi^{(n-k)} \tag{61}$$

Note that the problem of solving the higher order sensitivities is in essence, a lower-triangular problem, in the sense that the solution for the n-th order depends only on the solution of the orders $0, .., n-1$. We assume that our unknowns are ψ, λ, and all their higher order derivatives, and that we have knowledge of the operators F, and L, and all their higher order derivatives.

2.2.7 Solving the first-order problem

The equation we seek to solve is

$$L^{(1)}\psi + L\psi^{(1)} = \lambda^{(1)}F\psi + \lambda F^{(1)}\psi + \lambda F\psi^{(1)} \tag{62}$$

we begin by rearranging and grouping some terms

$$(L - \lambda F)\psi^{(1)} = \lambda^{(1)}F\psi + (\lambda F^{(1)}\psi - L^{(1)}\psi) \tag{63}$$

For the sake of clarity, lets define the operator $A \equiv (L - \lambda F)$, and lets also define $C_1 \equiv (\lambda F^{(1)}\psi - L^{(1)}\psi)$. So now we can write the equation in a more compact form:

$$A\psi^{(1)} = \lambda^{(1)}F\psi + C_1 \tag{64}$$

Here we can use the Fredholm alternative, which states that $\psi^{(1)}$ exists if and only if $\lambda^{(1)}F\psi + C_1$ is orthogonal to $Ker(A^\dagger)$. Since the dimension of $Ker(A^\dagger)$ is 1, and is spanned uniquely by the adjoint flux ϕ, it is enough to show that $\lambda^{(1)}F\psi + C_1$ is orthogonal to the adjoint flux ϕ to prove that a solution exists. The orthogonality implies that

$$< \lambda^{(1)}F\psi + C_1, \phi >= 0 \tag{65}$$

rearranging, we get a way to solve for $\lambda^{(1)}$

$$\lambda^{(1)} = -\frac{< C_1, \phi >}{< F\psi, \phi >} = -\frac{< (\lambda F^{(1)} - L^{(1)})\psi, \phi >}{< F\psi, \phi >} \tag{66}$$

This is exactly the ubiquitous first order perturbation theory equation.
Once we have $\lambda^{(1)}$, we can solve for $\psi^{(1)}$ by inverting A

$$\psi^{(1)} = A^{-1}(\lambda^{(1)}F\psi + C_1) \tag{67}$$

Solving for $\psi^{(1)}$
The equation for the derivative of flux, $\psi^{(1)}$, is the following

$$A\psi^{(1)} = \lambda^{(1)}F\psi + C_1 \tag{68}$$

The right hand side of the equation is known, the operator A is known and understood, plugging in the full definition of the operators we get

$$\Sigma_T(E)\psi^{(1)}(E) - \int_E^{E_\infty} \frac{\Sigma_s(E')}{E'}\psi^{(1)}(E')dE' - \lambda\chi(E)\int_{E_0}^{E_\infty} \nu\Sigma_f(E')\psi^{(1)}(E')dE'$$

$$= \lambda^{(1)}\chi(E)\int_{E_0}^{E_\infty} \nu\Sigma_f(E')\psi(E')dE' + \lambda\chi(E)\int_{E_0}^{E_\infty} \nu\Sigma_f^{(1)}(E')\psi(E')dE' - \Sigma_T^{(1)}\psi(E) + \int_E^{E_\infty} \frac{\Sigma_s^{(1)}(E')}{E'}\psi(E')dE' \tag{69}$$

Where the superscript (1) denotes the first derivative with respect to an arbitrary parameter x. This is just the neutron transport equation with a source term equivalent to the right hand side. We take the derivative of the equation with respect to energy to obtain a first order linear ordinary differential equation.

$$\frac{\partial \psi^{(1)}}{\partial E} + \left[\frac{\partial \ln \Sigma_t}{\partial E} + D_s(E)\right]\psi^{(1)} =$$

$$\left(\frac{\partial \chi}{\partial E}\right)\frac{1}{\Sigma_T}\left[\lambda \int_{E_0}^{E_\infty} \nu\Sigma_f(E')\psi^{(1)}(E')dE' + \lambda^{(1)}\int_{E_0}^{E_\infty} \nu\Sigma_f(E')\psi(E')dE' + \lambda \int_{E_0}^{E_\infty} \nu\Sigma_f^{(1)}(E')\psi(E')dE'\right]$$

$$- \frac{\Sigma_t^{(1)}}{\Sigma_t}\frac{\partial \psi}{\partial E} - \left(\frac{1}{\Sigma_t}\frac{\partial \Sigma_t^{(1)}}{\partial E} + \frac{\Sigma_s^{(1)}}{E\Sigma_t}\right)\psi \quad (70)$$

Notice that the right hand side contains the variable we are trying to solve for, $\psi^{(1)}$, however it is contained in an integral over all energy, therefore the value is just a constant and can be fixed by an additional boundary condition.

The solution to this equation takes the form

$$\psi^{(1)} = \frac{\int_E^{E_\infty} \mu(E')g(E')dE'}{\mu(E)} \quad (71)$$

where μ is the integrating factor given by

$$\mu(E) = \Sigma_t e^{\int D_s(E')dE'} \quad (72)$$

and $g(E)$ is the right hand side of the differential equation given by

$$g(E) = \left(\frac{\partial \chi}{\partial E}\right)\frac{1}{\Sigma_T}\left[\lambda \int_{E_0}^{E_\infty} \nu\Sigma_f(E')\psi^{(1)}(E')dE' + \lambda^{(1)}\int_{E_0}^{E_\infty} \nu\Sigma_f(E')\psi(E')dE' + \lambda \int_{E_0}^{E_\infty} \nu\Sigma_f^{(1)}(E')\psi(E')dE'\right]$$

$$- \frac{\Sigma_t^{(1)}}{\Sigma_t}\frac{\partial \psi}{\partial E} - \left(\frac{1}{\Sigma_t}\frac{\partial \Sigma_t^{(1)}}{\partial E} + \frac{\Sigma_s^{(1)}}{E\Sigma_t}\right)\psi \quad (73)$$

2.2.8 Solving the higher-order problem

Taking the equation for the n-th order derivative

$$\sum_{k=0}^{n}\binom{n}{k}L^{(k)}\psi^{(n-k)} = \sum_{k=0}^{n}\sum_{j=0}^{k}\binom{n}{k}\binom{k}{j}\lambda^{(j)}F^{(k-j)}\psi^{(n-k)} \quad (74)$$

it is possible to rewrite it in the form

$$A\psi^{(n)} = \lambda^{(n)}F\psi + C_n \quad (75)$$

If we define C_n as follows:

$$C_n = \sum_{j=0}^{n-1}\lambda^{(j)}F^{(n-j)}\psi + \sum_{k=1}^{n-1}\sum_{j=0}^{k}\binom{n}{k}\binom{k}{j}\lambda^{(j)}F^{(k-j)}\psi^{(n-k)} - \sum_{k=1}^{n}\binom{n}{k}L^{(k)}\psi^{(n-k)} \quad (76)$$

Notice that neither $\lambda^{(n)}$ nor $\psi^{(n)}$ appear in the definition of C_n. This allows us to use the Fredholm alternative once again to solve for $\lambda^{(n)}$.

$$\lambda^{(n)} = -\frac{< C_n, \phi >}{< F\psi, \phi >} \quad (77)$$

Higher order flux derivatives Going through the same steps as before, we obtain a solution for the flux derivatives

$$\psi^{(n)} = \frac{\int_E^{E_\infty} \mu(E')g_n(E')dE'}{\mu(E)} \tag{78}$$

Where the same integrating factor is used, the only difference is the g is replaced with g_n which is defined as

$$g_n(E) = \left(\frac{\partial\chi}{\partial E}\right)\frac{1}{\Sigma_T}\left[\lambda\int_{E_0}^{E_\infty}\nu\Sigma_f(E')\psi^{(n)}(E')dE' + \lambda^{(n)}\int_{E_0}^{E_\infty}\nu\Sigma_f(E')\psi(E')dE' + \right.$$

$$\sum_{j=0}^{n-1}\lambda^{(j)}\int_{E_0}^{E_\infty}\nu\Sigma_f^{(n-j)}(E')\psi(E')dE' + \sum_{k=1}^{n-1}\sum_{j=0}^{k}\binom{n}{k}\binom{k}{j}\lambda^{(j)}\int_{E_0}^{E_\infty}\nu\Sigma_f^{(k-j)}(E')\psi^{(n-k)}(E')dE' -$$

$$\left.\sum_{k=1}^{n-1}\binom{n}{k}\left[\frac{\Sigma_t^{(k)}}{\Sigma_t}\frac{\partial\psi^{(n-k)}}{\partial E} + \left(\frac{1}{\Sigma_t}\frac{\partial\Sigma_t^{(k)}}{\partial E} + \frac{\Sigma_s^{(k)}}{E\Sigma_t}\right)\psi^{(n-k)}\right]\right. \tag{79}$$

2.2.9 Taylor expansion of $\lambda(x)$

Having obtained the derivatives of λ with respect to some parameter x, it is now trivial to perform a Taylor expansion of $\lambda(x)$ around some reference value x_{ref}

$$\lambda(x) = \sum_{n=0}^{\infty}\frac{\lambda^{(n)}}{n!}(x - x_{ref})^n \tag{80}$$

3 Embedded Monte Carlo

We here present the results of our work investigating a random walk in a random environment method to propagate nuclear data uncertainty across neutron transport simulations, the results of which were presented at the M&C conference under the article [4], which we here transcribe. In addition, an extension of this work is the subject of an article that will be submitted soon.

3.1 Introduction to nuclear data uncertainty propagation

Nuclear cross sections $\sigma(E)$ are evaluated empirically as a function of the energy E of the impinging particle [5][6]. The values are reported in evaluated nuclear data files (ENDF [7], JEFF, JENDL, etc.) along with their *epistemic uncertainty*. This uncertainty is modeled and documented as a normal distribution on the resonance energies E_λ and widths $\gamma_{\lambda,c}$, which we shall henceforth collectively denote symbolically as the $\{\Gamma\}$ vector, that parameterize the R-matrix models of the quantum nuclear interaction cross sections: $\sigma_\Gamma(E)$, with $\Gamma \sim \mathcal{N}\Big(\Gamma_0, \mathbb{V}\mathrm{ar}\left[\Gamma\right]\Big)$.

$$\begin{aligned}\Gamma_0 &\triangleq \mathbb{E}_\Gamma\left[\Gamma\right] \\ \mathbb{V}\mathrm{ar}\left(\Gamma\right) &\triangleq \mathbb{E}_\Gamma\left[\left(\Gamma - \Gamma_0\right)\left(\Gamma - \Gamma_0\right)^\top\right]\end{aligned} \tag{81}$$

When propagated across Monte Carlo nuclear transport codes, this initial empirical uncertainty can result in very significant error-bars on the outputs of the Monte Carlo calculations, up to more than 1000pcm, or 1-4% of the power in a simple light water reactor model [8]. Accurately quantifying this epistemic uncertainty on the output of nuclear Monte Carlo transport solvers is thus crucial not only for the analyst but also to focus the efforts in improving the nuclear data.

Among others [9][10][11], two methods have been widely adopted to this effect: sensitivity analysis; and Total Monte Carlo. *Sensitivity analysis* perturbs inputs and computes the first order effect on the output. This requires tallying the derivatives of the inputs with respect to the inputs, itself an endeavor [12, 13]. *Total Monte Carlo* is much more straightforward, but computationally expensive [14, 3]. It samples the

inputs from their distribution, $\Gamma \sim \mathcal{N}\Big(\mathbb{E}\left[\Gamma\right], \mathbb{V}\mathrm{ar}\left[\Gamma\right]\Big)$, and runs a full Monte Carlo $\mathbb{MC}$ transport solve for each Γ realization. The outputs histogram distribution is then estimated to derive confidence intervals.

$$\mathrm{Hist}\left[R_i(E), k_{\mathrm{eff}}\right] = \mathrm{Hist}_{\Gamma}\left[\mathbb{MC}\big[\Gamma\big]\right] \tag{82}$$

If each Monte Carlo $\mathbb{MC}$ run requires N neutrons to converge, and M occurrences of resonance parameters Γ are sampled, then Total Monte Carlo now requires N×M neutrons. To diminish this gargantuan computational requirement, Zwermann and Rochman proposed the fast-Total Monte Carlo (fast-TMC) method [15, 3], which cuts down the total number of neutrons run to N by simply running M simulations of N/M neutrons, but care must be taken in large realistic system susceptible to clustering or under-sampling. If the total number of neutrons that can be run is fixed, fast-TMC marks a trade-off between the statistical power to resolve the aleatoric uncertainty within each batch, and the statistical power to resolve the epistemic uncertainty between each batch. Rochman proposed the heuristic independence of variances in equation (4) of [3] to estimate this trade-off:

$$\sigma^2_{\mathrm{observed}} \approx \sigma^2_{\mathrm{statistics}} + \sigma^2_{\mathrm{epistemic}} \tag{83}$$

3.2 Embedded Monte Carlo: Random walk in Random environment

This article studies the limits of TMC as we sample the epistemic uncertainty within the Monte Carlo neutron random walk, and explores the alternative methods to propagate epistemic uncertainty across a nuclear Monte Carlo transport simulation. We do this by embedding the epistemic uncertainty within the Monte Carlo random walk, thus running a new random walk in a random cross section environment.

3.2.1 Stochastic Nuclear Cross Sections

The key to being able to do this is to represent the empirical uncertainty on nuclear cross sections as a function of energy (and temperature for Doppler broadening) parametrized with an epistemic stochastic variable Γ, thereby creating stochastic cross sections:

$$\sigma_{\Gamma}(E,T) = \mathbb{A}^{\mathrm{Quantum}}_{\mathrm{Temperature}}\Big(E, T \mid \Gamma\Big) \qquad , \qquad \Gamma \sim \mathcal{N}\Big(\mathbb{E}\left[\Gamma\right], \mathbb{V}\mathrm{ar}\left[\Gamma\right]\Big) \tag{84}$$

where T is the temperature of the target. Figure 9 gives an example of various $T = 0$K samples of such stochastic cross sections (84).

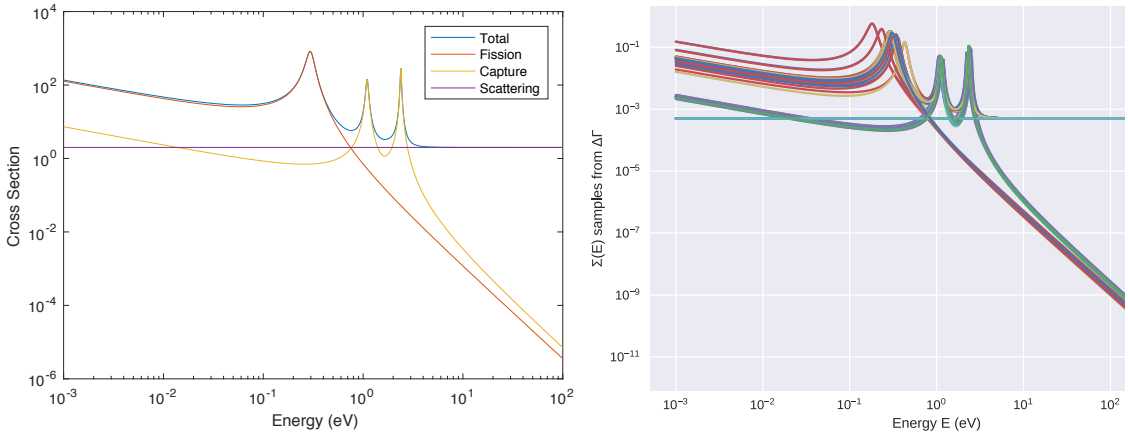

(a) Mean cross sections

(b) Samples from stochastic cross section

Figure 9: Example of mean and stochastic cross sections, generated from Normal-sampling of the mean $\mathbb{E}\left[\Gamma\right]$, and co-variance $\mathbb{V}\mathrm{ar}\left[\Gamma\right]$ matrix of the resonance parameters.

3.2.2 Embedded cross section sampling within the Monte Carlo transport

Representing the cross section as a stochastic variable (84) allows us to sample the cross sections at any point in the Monte Carlo simulation. This sampling can be done at three levels, as represented in algorithm 1: (1)

Batch Embedded Monte Carlo (b-EMC): at each batch of neutrons (this in effect is similar to fast-TMC); (2) *Neutron Embedded Monte Carlo* (n-EMC): at each new neutron (equivalent to a batch of 1); (3) *Collision Embedded Monte Carlo* (c-EMC): at each new collision of the neutron random walk.

Intuitively, we can think of Total Monte Carlo (TMC) as a standard Monte-Carlo propagation through a deterministic solution, that is an outer epistemic loop on Γ is run atop a code that generates the conditional values, say $k_{\text{eff}}|\Gamma$. On the other hand, Embedded Monte Carlo (EMC) is a new random walk in a random environment for the neutron: neutrons evolve in an environment where the physics are uncertain.

for *each batch b* **do**
  sample stochastic cross section $\sigma_\Gamma(E,T)$ from (84) ← Batch Sampling (b-EMC) ;
  for *each neutron n in batch b* **do**
    sample stochastic cross section $\sigma_\Gamma(E,T)$ from (84) ← Neutron Sampling (n-EMC) ;
    while *neutron is alive* **do**
      sample stochastic cross section $\sigma_\Gamma(E,T)$ from (84) ← Collision sampling (c-EMC) ;
      collide with cross sections $\sigma_\Gamma(E,T)$ and transport;
      Perform tallies: k_{eff}, collisions and squared $\text{Col}(E_g)$, $\text{Col}^2(E_g)$, for energy groups E_g ;
    end
  end
end

Algorithm 1: Embedded Monte Carlo Algorithm: three possible levels of embedded sampling

Mathematically, the expectation value of the neutron random walk (no uncertainty on the cross sections) is a solution to the Boltzmann transport equation [16][17]. TMC then looks at how these solutions differ for each new input. EMC proposes different random walks, their expectation values are not guaranteed *a priori* to solve the Boltzmann equation. b-EMC can be seen as fast-TMC with only one Monte Carlo (MC) run per batch. n-EMC is akin to the limit-case of one neutron per batch. c-EMC can be though of in analogy with Doppler-broadening similarly to the target motion sampling approach in Serpent in that for each new collision it samples a new realization of a possible cross section given our uncertainty, just like we can sample a target velocity from the Maxwell distribution [12][18]. However, c-EMC also appears intuitively un-physical, as the R-matrix equations entail strong correlations within the cross section $\sigma_\Gamma(E,T)$, which would be lost by such collision-embedding.

3.2.3 Definitions and notations

In order to study the capabilities that Embedded Monte Carlo can offer for uncertainty quantification, we must first set the framework of the problem. Let us first introduce the notation and define quantities of interest, along with their estimators.

Definitions:

Let $\mathbb{E}_{\text{MC}}[\cdot]$ be the expectation value from the Monte Carlo random walk. For sake of simplicity, we will focus the analysis on the k_{eff} eigenvalue, though the results are applicable to any tally. There are different quantities of interest to us in this study:

- $k(\Gamma)$: the expected k_{eff} from a Monte Carlo run, given the set of resonance parameters Γ as an input, that is:
$$k(\Gamma) \triangleq \mathbb{E}_{\text{MC}}[k|\Gamma] \tag{85}$$
- k_0: the value of k_{eff} when running the neutron random walk with the mean resonance parameters Γ_0, that is $k_0 \triangleq k(\Gamma_0)$ where $\Gamma_0 \triangleq \mathbb{E}_\Gamma[\Gamma]$, i.e. $k_0 = \mathbb{E}_{\text{MC}}[k|\Gamma_0] = \mathbb{E}_{\text{MC}}[k|\mathbb{E}_\Gamma[\Gamma]]$.
- $\langle k\rangle_\Gamma$: the expectation value of $k(\Gamma)$ given the distribution of Γ, that is:
$$\langle k\rangle_\Gamma \triangleq \mathbb{E}_\Gamma[k(\Gamma)] \tag{86}$$
  In other words, given our epistemic uncertainty distribution on Γ, this quantity represents the expectation value of k_{eff} over all the possible values of Γ.
- $\mathbb{V}\text{ar}_\Gamma(k)$: the variance of $k(\Gamma)$ given the distribution of Γ, that is:
$$\mathbb{V}\text{ar}_\Gamma(k) \triangleq \mathbb{E}_\Gamma\left[\left(k(\Gamma) - \langle k\rangle_\Gamma\right)^2\right] = \mathbb{E}_\Gamma\left[k(\Gamma)^2\right] - \mathbb{E}_\Gamma\left[\langle k\rangle_\Gamma\right]^2 \tag{87}$$

This represents the variance of $k(\Gamma)$ around its mean $\langle k \rangle_\Gamma$ given our epistemic uncertainty distribution on Γ.

Estimators definitions:
Let N_{tot} be the total number of neutrons, B be the number of batches, and $N_B \triangleq N_{\text{tot}}/B$ be the number of neutrons per batch. We will define the following estimators:

- $\overline{k}_b^{\text{MC}} \triangleq \frac{1}{N_B} \sum_{n=1}^{N_B} k_n|\Gamma_0$: the batch k_{eff} mean estimator, that is the average of all the $k_n|\Gamma_0$ values in the batch (in our analog Monte Carlo case, k_n is either ν or 0 for each neutron), given the mean resonance parameters Γ_0.
- $\overline{k}_{\text{eff}}^{\text{MC}} \triangleq \frac{1}{B} \sum_{b=1}^{B} \overline{k}_b^{\text{MC}}$: the mean of batch k_{eff} means estimator.
- $\Delta\overline{k}_{\text{eff}}^{\text{MC}} \triangleq \frac{1}{B-1} \sum_{b=1}^{B} \left(\overline{k}_b^{\text{MC}} - \overline{k}_{\text{eff}}^{\text{MC}}\right)^2$: the variance of batch means estimator, that is the the (unbiased) average of all the $\left(\overline{k}_b - \overline{k_{\text{eff}}}\right)^2$ square-distances between the means of each batch.
- $\overline{k}_{\text{eff}}^{\text{b-EMB}} \triangleq \frac{1}{B} \sum_{b=1}^{B} \overline{k}_b|\Gamma$: the mean of batch k_{eff} means estimator, where each batch mean $\overline{k}_b|\Gamma$ is estimated with a different Γ, sampled from $\Gamma \sim \mathcal{N}\Big(\mathbb{E}\left[\Gamma\right], \mathbb{V}\text{ar}\left[\Gamma\right]\Big)$ to compute cross sections (84).
- $\Delta\overline{k}_{\text{eff}}^{\text{b-EMB}} \triangleq \frac{1}{B-1} \sum_{b=1}^{B} \left(\overline{k}_b|\Gamma - \overline{k}_{\text{eff}}^{\text{b-EMB}}\right)^2$: the corresponding variance of the batch means.
- $\overline{k}_b^{\text{n-EMB}} \triangleq \frac{1}{N_B} \sum_{n=1}^{N_B} k_n|\Gamma$: the batch mean k_{eff} estimator, where each neutron sample $k_n|\Gamma$ is run with a different Γ, sampled from $\Gamma \sim \mathcal{N}\Big(\mathbb{E}\left[\Gamma\right], \mathbb{V}\text{ar}\left[\Gamma\right]\Big)$ to compute cross sections (84).
- $\overline{k}_{\text{eff}}^{\text{n-EMB}} \triangleq \frac{1}{B} \sum_{b=1}^{B} \overline{k}_b^{\text{n-EMB}}$: the corresponding mean of batch k_{eff} means estimator for neutron-sampling Embedded Monte Carlo.
- $\Delta\overline{k}_{\text{eff}}^{\text{n-EMB}} \triangleq \frac{1}{B-1} \sum_{b=1}^{B} \left(\overline{k}_b^{\text{n-EMB}} - \overline{k}_{\text{eff}}^{\text{n-EMB}}\right)^2$: the corresponding variance of the batch means.
- $\overline{k}_b^{\text{c-EMB}}$, $\overline{k}_{\text{eff}}^{\text{c-EMB}}$, $\Delta\overline{k}_{\text{eff}}^{\text{c-EMB}}$ can all be defined analogously, using $k_n^{\text{c-EMB}} \triangleq k_n\|\Gamma_{\text{collision}}$, where we now sample new Γ values from $\Gamma \sim \mathcal{N}\Big(\mathbb{E}\left[\Gamma\right], \mathbb{V}\text{ar}\left[\Gamma\right]\Big)$ to compute cross sections (84) at each collision during the random walk of each individual neutron.

3.2.4 Theoretical Considerations

Propagating the resonance parameters $\{\Gamma\}$ epistemic uncertainty across the neutron transport problem is in effect the study of the distribution of $k(\Gamma)$ given the distribution of Γ, that is the histogram of equation (82). This represents how much the mean outputs from the Monte Carlo particle transport vary due to our uncertainty of the nuclear physics (84).

Bernoulli statistics
In a fully analog Monte-Carlo simulation with constant ν, each neutron is born, and will collide for each reaction-rate tally, contributing in the end ν neutrons for fission events, or zero for all other collisions. This means that all the estimators are Bernoulli variables. For instance, if p is the probability of fissioning, and assuming the number of neutrons constant per fission, each neutron will have a multiplication factor of ν or 0: $k_n \sim \nu p + 0(1-p)$. The expectation value is then the multiplication factor: $k_{\text{eff}} \triangleq \mathbb{E}\left[k_n\right] = \nu p$. The average tallies over any group of neutrons will slowly converge towards a Gaussian distribution, as proved by the de Moivre-Laplace theorem [19][20], and here illustrated in figure 10.

Since all tallies are Bernoulli variables, this also means the variance is: $\Delta k_{\text{eff}} \triangleq \mathbb{V}\text{ar}\left[k_n\right] = \mathbb{E}\left[k_n^2\right] - k_{\text{eff}}^2 = \frac{1}{\nu^2} p(1-p) = k_{\text{eff}}(\nu - k_{\text{eff}})$. This is true of all cases, simple MC (no uncertainty), b-EMC, n-EMC, or c-EMC, and can be verified numerically by comparing the numerical variance from table 1 to the variance calculated from the theoretical Bernoulli relation $\Delta k_{\text{eff}} = k_{\text{eff}}(\nu - k_{\text{eff}})$, using the numerical k_{eff} values from table 1: one will note both variances match perfectly to up to 10 digits. The fact that $\Delta k_{\text{eff}} = k_{\text{eff}}(\nu - k_{\text{eff}})$ is a quadratic function of k_{eff} entails that it takes its maximum value for the special case of $\nu = 2$, $k_{\text{eff}} = 1$. This leads to the very counter-intuitive result that if the no-uncertainty sampling MC run is performed on this case, we will

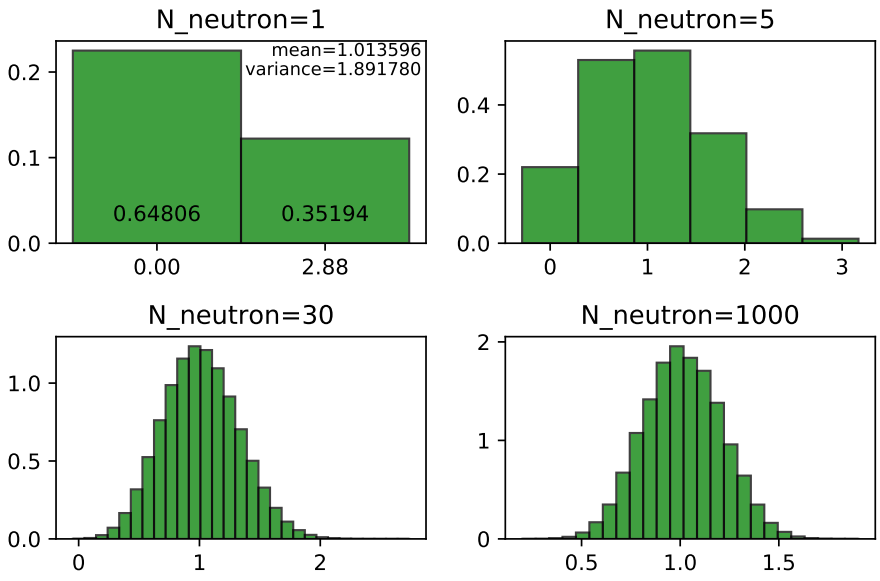

Figure 10: Histogram of batch keffs: demonstrating the Bernoulli distribution

obtain a variance of 1, but if we start adding stochastic cross sections for epistemic uncertainty (assuming ν is fixed), this will necessarily lead to a lower variance, regardless of whether $k_{\text{eff}}^{\text{b-EMC,n-EMC}}$ increased or not. This counter-intuitive behavior is shown in the results hereafter documented in table 1.

3.3 Results and Analysis

To study these different schemes, we devised a set of numerical experiments to cast a light on different theoretical considerations.

Experimental setup:
We designed two 0K slowing-down problems for which we have constructed an analytic benchmark [1], and ran each of them with two different covariance matrices that differ in magnitude Cov(Γ) for the epistemic uncertainties. The goal was to detect the departure from linear behavior in the resonance parameters perturbations around the mean. This leads to a total of four different cases. Both benchmarks are specified as a pure slowing-down problem in the presence of the first resonances of U^{238} and Pu^{239}. The specific resonance parameters values and covariances are detailed in **??**. The first benchmark has $\nu = 2.88$, while the second benchmark was designed to achieve the particular case of $\nu = 2$ and $k_{\text{eff}} = 1$. This was done in order to better illustrate the argument on the Bernoulli distributions explained in the theoretical considerations section 3.2.4.

To run these four different cases, we coded a simple analogous Monte Carlo slowdown code, which can be found at: `https://github.com/mit-crpg/Embedded_Monte_Carlo`. Selected key values for the four studies are here documented in table 1.

Expectation values measurements:
A priori, the means from Embedded Monte Carlo, $\overline{k}_{\text{eff}}^{\text{b-EMB}}$, $\overline{k}_{\text{eff}}^{\text{n-EMB}}$, and $\overline{k}_{\text{eff}}^{\text{c-EMB}}$, should all be different from the $\overline{k}_{\text{eff}}^{\text{MC}}$ obtained from the mean resonance parameters Γ_0, with no epistemic uncertainty. To illustrate this, we ran the analytic benchmark with one billion neutrons, and recorded the results for different ways of sampling and batching, as plotted in Figure 11.

One can observe that the b-EMC mean is the same as the n-EMC mean, $\overline{k}_{\text{eff}}^{\text{b-EMB}} = \overline{k}_{\text{eff}}^{\text{n-EMB}}$, both of which differ from the no-epistemic uncertainty mean $\overline{k}_{\text{eff}}^{\text{MC}}$. This shows that to obtain the same mean as the b-EMC, one only needs to run one neutron per batch. Indeed, n-EMC and b-EMC are identical at one neutron per batch. However b-EMC suffers from batch-undersampling, while the n-EMC does not. This can be seen in figure 11, where we can observe at least 10^4 batches are needed to converge the batch estimators, below

Table 1: Key values for different embedded sampling schemes in the numerical Monte Carlo experiments

Model	Sampling scheme	Neutrons per batch	Covariance matrix	Mean of k ($\overline{k}_{\text{eff}}$ estimator)	Variance of k means ($\Delta\overline{k}_{\text{eff}}$ estimator)
ν=2.88	no sampling	1	none	1.00002	1.88002
ν=2.88	no sampling	1000	none	0.99995	0.00188
ν=2.88	sampling per batch	1	small	1.00078	1.88068
ν=2.88	sampling per batch	1000	small	1.00077	0.00228
ν=2.88	sampling per batch	1	large	1.01359	1.89177
ν=2.88	sampling per batch	1000	large	1.01361	0.03932
ν=2.88	sampling per neutron	1	large	1.01359	1.89177
ν=2.88	sampling per neutron	1000	large	1.01359	0.00189
ν=2.88	sampling per collision	1	large	1.01807	1.89557
ν=2.88	sampling per collision	1000	large	1.01769	0.00190
ν=2.0	no sampling	1	none	1.00002	1.00000
ν=2.0	no sampling	1000	none	1.00000	0.00099
ν=2.0	sampling per batch	1	small	1.00016	0.99999
ν=2.0	sampling per batch	1000	small	1.00017	0.00110
ν=2.0	sampling per batch	1	large	1.00126	0.99999
ν=2.0	sampling per batch	1000	large	1.00128	0.01744

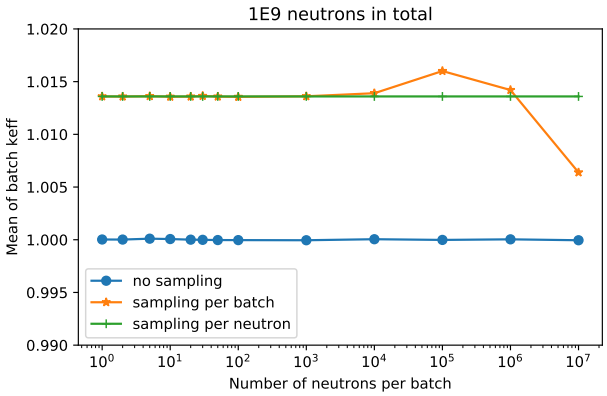

(a) Mean of batch $\overline{k}_b$

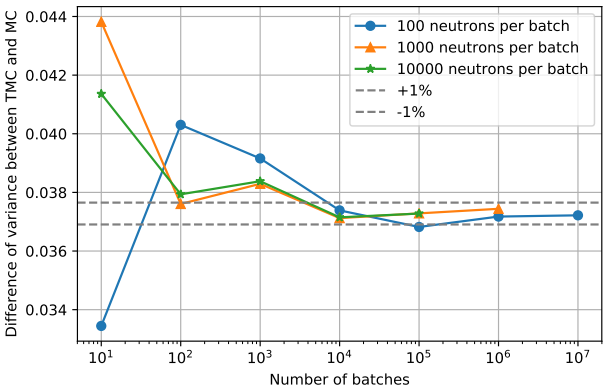

(b) $\overline{k}_b$

Figure 11: b-EMC and n-EMC means are the same, and different from MC. However, 10^4 batches are necessary to converge b-EMC epistemic variances.

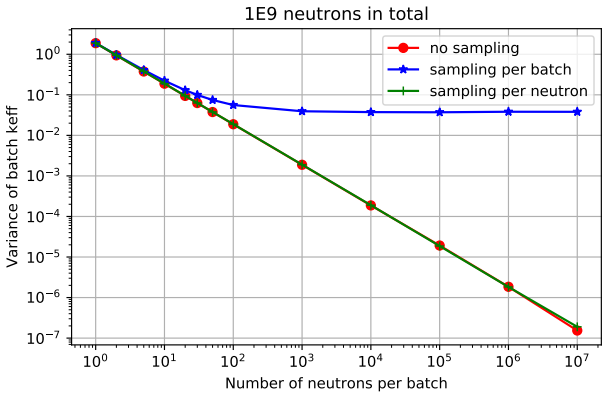

(a) Variance of batch $\overline{k}_b$

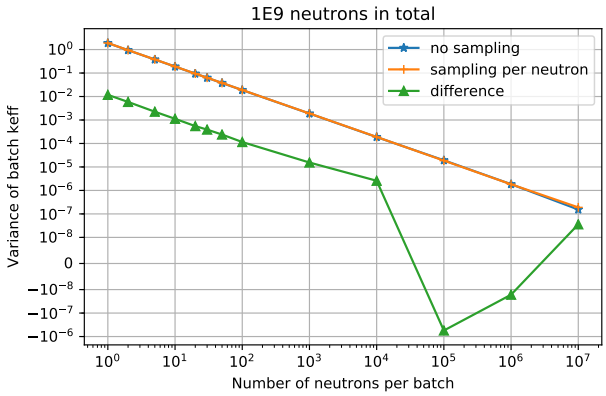

(b) MC v.s. n-EMC difference $\overline{k}_b$

Figure 12: MC and b-EMC Variances add up as in equation (83) only for enough neutrons per batch. n-EMC and MC variances are different and do not add up.

this number of batches the error bars on the batch-estimators are very large, hence the large fluctuations observed. This shows the statistical-power trade-off between batch-level statistics and neutron-level statistics in b-EMC (which is the same as TMC).

From table 1, we also observe that $k(\Gamma)$ is not linear, even at small perturbations around Γ_0. Indeed, there is always a difference between $\overline{k}_{\text{eff}}^{\text{b-EMB}} = \overline{k}_{\text{eff}}^{\text{n-EMB}}$ and $\overline{k}_{\text{eff}}^{\text{MC}}$, which is smaller with the covariance matrix.

One can also observe from table 1 that the c-EMC random walk with sampling per collision yields a different mean $\overline{k}_{\text{eff}}^{\text{c-EMB}}$ than either MC, TMC or EMC. There is about 1800pcm difference with $k_{\text{eff}}^{\text{MC}}$, and some 450pcm difference with $k_{\text{eff}}^{\text{TMC}} = k_{\text{eff}}^{\text{EMB}}$. This most likely indicates that collision sampling is physically incorrect, as our heuristic argument on the energy-level correlations advocated.

Variance measurements:
The numerical experiments on the means discarded the c-EMC scheme, and showed b-EMC and n-EMC to have the same mean. We thus searched for ways to extract the epistemic uncertainty from the n-EMC scheme. In particular, if Rochman's heuristic equation (83) stands to the limit of one-neutron per batch, then it could be that one could run two cases: one MC without uncertainty propagation, and then one n-EMC case. The direct subtraction of the variances of the latter two would then be the variance from the epistemic uncertainty.

To test the veracity of such result, we computed the difference between the variances of the batch k_{eff} obtained from the no-sampling MC, the b-EMC, and the n-EMC, and documented the results in Figure 12. One can observe that the variances of the b-EMC plateaus past a certain amount of neutrons per batch (about 10^4), while the variances of the n-EMC and the MC process are different by a constant.

This prompted us to study the differences in theses variances, to see if indeed we could add them up. Unfortunately, Figure 13 tells a more complicated story. It shows the differences in the variances between the b-EMC and the MC cases, and one can observe that the difference between the MC and the b-EMC variances is constant past 100 neutrons per batch. It is thus possible to run two cases, one MC and one b-EMC, and subtract them to obtain the epistemic uncertainty. However, this behavior breaks down when we tend towards the n-EMC limit of one neutron per batch.

More precisely, we observe that Rochman's equation (83) is valid only for enough neutrons per batch in b-EMC. Figure 12 shows b-EMC needs at least 1000 neutrons per batch to converge the batch means. This can be interpreted as the need to converge each batch's Bernoulli means to Gaussian, which requires about 1000 tallies, as illustrated in Figure 10. Furthermore, Figure 11 shows b-EMC needs at least 10000 batches to resolve the epistemic uncertainty. We are thus still observing the epistemic v.s. aleatoric statistical power trade-off exhibited by Rochmann in [3].

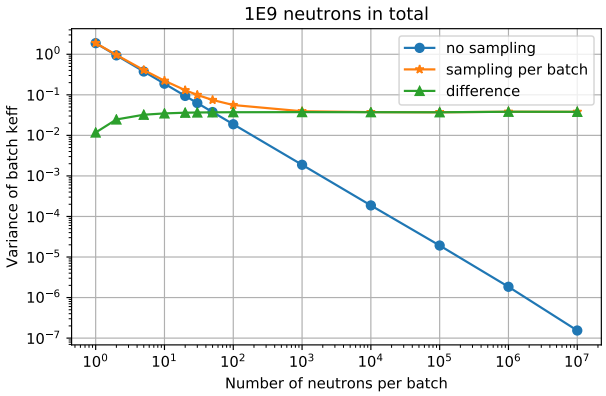

(a) Differences in variance of batch $\overline{k}_b$

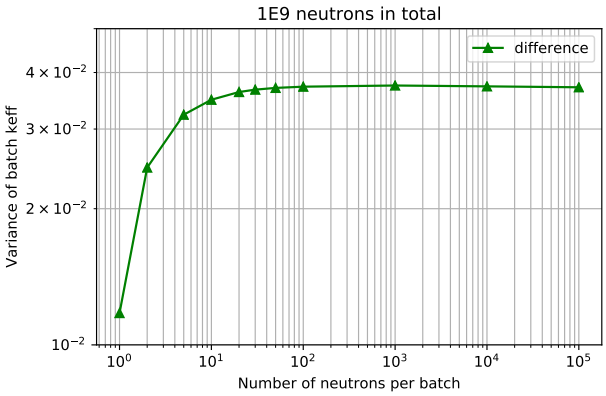

(b) Zooming-in

Figure 13: MC v.s. b-EMC and n-EMB: when variances do not add up as in equation (83).

3.4 Conclusions on Embedded Monte Carlo

This study examined the possibility of embedding cross section sampling in the random walk in order to estimate the epistemic uncertainty. The simple test case leads us to the following conclusions:

- Collision-sampling Embedded Monte Carlo (c-EMC) is incorrect: or at least we do not know what the results correspond to nor solve for. Moreover, it is prohibitively computationally expensive.
- The neutron-sampling Embedded Monte Carlo (n-EMC) mean converges to the mean from batch-sampling Embedded Monte Carlo (b-EMC). n-EMC has the advantage of having much stronger statistics (no under-sampling of the epistemic). However, sampling at each neutron can be quite costly.
- The n-EMC variance does not add up to the b-EMC variance of means plus the MC (no sampling) variance of means. It is still an open question to find a way to extract the epistemic variance from the aleatoric one in n-EMC. However, we have found away of combining a fast-TMC with an neutron Embedded Monte Carlo to do so, thereby overcoming the undersampling problem of fast-TMC. This will be the subject of a coming article.
- Since all variables are Bernoulli in the analog case studied, b-EMC just needs enough neutrons per batch to converge the mean of the Bernoulli distribution. This is a direct application of the Moivre-Laplace theorem [19][20]. We observe than 1000 counts is enough. This is more than it seems, because the multiplication factor k_{eff} is an integral quantity over energies. This means that for energy-dependent reaction rates 1000 counts is harder to achieve for every "box" of an energy grid (specially when reaction rates probabilities are low). However, we also observed that we can gain one order of magnitude on the number of neutrons needed by running the problem twice, once with b-EMC and once without sampling MC, and taking the difference: 100 counts in then enough to make sure the difference reveals the epistemic uncertainty.

4 Sensitivity based Monte Carlo

We here present the results of our work implementing sensitivities to multipole parameters in OpenMC, the results of which were presented at the M&C conference, which we here transcribe. Since this paper was published, the capability was extended to leverage CLUTCH and CLUTCH-FM to calculate the adjoint-weighted tallies. Additionally, current work is being focused on enabling multithreading for this capability.

4.1 Introduction

Predictive simulations of existing and future nuclear designs has been a major area of research in the past couple of decades. As the cost, and difficulty, of performing nuclear experiments increases, it has become

more important to develop accurate simulation tools to model and predict the behavior of new designs. Monte Carlo methods in neutron transport are seen as a vital tool in this effort due to their high fidelity and accurate representation of the physics. Uncertainties arrising from nuclear data are a major source of uncertainty in the results of these Monte Carlo simulations, and thus it is important to quantify these uncertainties, and point towards ways of decreasing it.

Accurate evaluated nuclear cross section data are needed for radiation transport calculations for nuclear applications. In the cross section evaluation procedure, data evaluators attempt to fit the nuclear physics model to measured differential data by selecting and manipulating the resonance parameters that parametrize the formulation of the cross sections. The model, which can be derived from quantum scattering theory, results in an equation for the cross section of the form

$$\sigma(E) = f(E; \mathbf{\Gamma}) \tag{88}$$

where $\mathbf{\Gamma}$ are the resonance parameters. It is ultimately these resonance parameters that define the interactions of the nuclei. The process of differential evaluation of the resolved resonance region is a mathematically overdetermined problem with no exact solution. Therefore, there is much choice left to the evaluator in seeking parameters that minimize a certain metric. Even once an evaluation is considered complete based on differential experimental data, it is not unique, and other possibilities exist that may satisfy the metrics used to determine the accuracy of the evaluation. Simply put, the experimentally measured cross section value at every energy point is reported only as a mean value and a standard deviation. Therefore, it is statistically equivalent for the cross section reconstructed from the resonance parameters, Γ, to pass above or below the mean experimental value by the same amount. This ambiguous choice previously has been left to the evaluator's discretion.

Much of the systematic uncertainty on differential cross section data comes from the normalization of capture and inelastic cross section measurements. These measurements demand that the experimenter has a high degree of knowledge of the experimental flux; unfortunately, this is not always the case. In the best case, this results in larger uncertainties over certain energy regions of the experimental data. In the worst case, the experimental cross section data is misreported. This can be manifested in systematically larger or smaller mean values for the measured cross section or small uncertainty that does not reflect the actual state of knowledge. Unlike statistical uncertainty, systematic uncertainty can result in resolved resonance evaluations that produce a cross section that is too high over a large energy region. Therefore, the uncertainty on the normalization of experimental data is one of the biggest concerns in completing a new evaluation of a resolved resonance region based on differential experimental data.

When simulating the neutronics of a nuclear system, the uncertainty in the nuclear data constitutes one of the two major sources of uncertainty in the results of the simulation, the other being the errors introduced by the calculation scheme. The calculation scheme can effectively be driven to arbitrarily small values by either running more particles in Monte Carlo, or refining the phase space in a deterministic calculation. On the other hand, the uncertainties stemming from nuclear data cannot be reduced without revising the underlying nuclear data evaluations, and must thus be accounted for when conducting a reactor physics calculation. In the case of Monte Carlo neutronics calculations, which are often used as reference solutions for deterministic codes, nuclear data uncertainties propagated through the reactor core calculation make-up the bulk of the uncertainties. For instance, recent studies have shown that, in the case of the OECD/NEA Martin-Hoogenboom benchmark, the single propagation of ^{235}U, ^{238}U, ^{239}Pu cross section uncertainties and that of the H and H_2O thermal scattering $S(\alpha, \beta)$ kernels yield local fission pin power uncertainties at mid-height ranging between 1% (in the center of the core) to 4% (at the periphery), while the statistical uncertainty of the Monte Carlo simulation was always well below 1% [8].

4.2 Windowed Multipole Formalism

The multipole formalism [21, 22, 23, 24, 25, 26, 2, 27, 28] is in essence a mathematical reformulation of the cross section in terms of new parameters, poles and residues. The reformulation comes from a partial fraction decomposition of the Reich-Moore cross section formula. In the multipole formalism, the cross section at $0K$ can be expressed as:

$$\sigma(E) = \frac{1}{E} \sum_j \Re \left[\frac{r_j}{p_j - \sqrt{E}} \right] \tag{89}$$

The advantage we gain from using the multipole formalism shows itself when Doppler broadening the cross section

$$\sigma(E,T) = \frac{1}{2E\sqrt{\xi}} \sum_j \Re \left[ir_j \sqrt{\pi} W(z) - \frac{r_j}{\sqrt{\pi}} C\left(\frac{p_j}{\sqrt{\xi}}, \frac{\sqrt{E}}{2\sqrt{\xi}} \right) \right] \tag{90}$$

Where

$$\xi = \frac{k_b T}{4A}$$

$$z = \frac{\sqrt{E} - p_j}{2\sqrt{\xi}}$$

Where W is the Faddeeva function, a function for which numerous high performance evaluators are available, and C has been found to be so small that it can be safely ignored. The implication of this is that it now becomes feasible to perform doppler broadening on-the-fly. So the equation can be approximated using

$$\sigma(E,T) = \frac{1}{2E\sqrt{\xi}} \sum_j \Re \left[ir_j \sqrt{\pi} W(z) \right] \tag{91}$$

The sum over all the poles is an expensive operation, computationally. However, one can notice that one can consider only the poles that are in some neighborhood of energy E, and all other poles that are far away can be approximated using a polynomial curve fit.

$$\sigma(E) = \frac{1}{E} \sum_{j \in w} \Re \left[\frac{r_j}{p_j - \sqrt{E}} \right] + \frac{1}{E} \sum_n c_n \sqrt{E}^n \tag{92}$$

Where w is the window, and the sum of the polynomial is typically taken over 3 terms. The polynomials have well known doppler broadened forms. The ability to doppler broaden on-the-fly enables us to propagate the uncertainty in nuclear data in a much better way than could ever be possible using the traditional Reich-Moore formalism of cross sections.

4.2.1 Derivatives with respect to pole parameters

We would now like to take the derivative of the cross section with respect to the multipole parameters. Since the parameters are complex numbers, we must take the derivative with respect to the real and imaginary part separately. One of the most useful aspects of the multipole formalism is evident when taking the derivatives, and that is the independence of individual poles.

Starting with the zero-K form of the cross section, we see that

$$\frac{\partial \sigma}{\partial \Re r_k} = \frac{1}{E} \Re \left[\frac{1}{\sqrt{E} - p_k} \right] \tag{93}$$

$$\frac{\partial \sigma}{\partial \Im r_k} = \frac{1}{E} \Im \left[\frac{1}{\sqrt{E} - p_k} \right] \tag{94}$$

$$\frac{\partial \sigma}{\partial \Re p_k} = \frac{1}{E} \Re \left[\frac{r_k}{(\sqrt{E} - p_k)^2} \right] \tag{95}$$

$$\frac{\partial \sigma}{\partial \Im p_k} = \frac{1}{E} \Im \left[\frac{r_k}{(\sqrt{E} - p_k)^2} \right] \tag{96}$$

The derivatives of the doppler-broadened cross sections are

$$\frac{\partial \sigma}{\partial \Re r_k} = \frac{1}{2E\sqrt{\xi}} \Re \left[\sqrt{\pi} W(z_k) \right] \tag{97}$$

$$\frac{\partial \sigma}{\partial \Im r_k} = \frac{1}{2E\sqrt{\xi}} \Re \left[i\sqrt{\pi} W(z_k) \right] \tag{98}$$

$$\frac{\partial \sigma}{\partial \Re p_k} = \frac{1}{2E\xi} \Re \left[r_k \left(1 + \sqrt{\pi} z_k W(z_k) \right) \right] \tag{99}$$

$$\frac{\partial \sigma}{\partial \Im p_k} = -\frac{1}{2E\xi} \Re \left[i r_k \left(1 + \sqrt{\pi} z_k W(z_k) \right) \right] \tag{100}$$

4.3 Current Sensitivity Methods

The current state of the art in nuclear data uncertainty propagation is based on the so called "sandwich formula." In this method, the cross section covariance matrix is sandwiched with the cross section sensitivity coefficients. The uncertainty, δR, in the quantity R can be expressed as:

$$\delta R = S_\sigma^R C_{\sigma\sigma} S_\sigma^{R^T} \tag{101}$$

Where the sensitivity coefficient, S_σ^R is defined as:

$$S_\sigma^R = \frac{\partial R/R}{\partial \sigma/\sigma} \tag{102}$$

This sensitivity coefficient can be calculated in the MCNP, Serpent, and SCALE codes using various methods such as IFP[29], CLUTCH[13], and the collision-history method.

4.3.1 Utilization of continuous energy Monte Carlo

The sensitivity, S_σ^R can be calculated using continuous energy monte carlo, however, in order to use the sandwich formula, this sensitivity has to be binned into an energy group structure. A finer group structure will approach the accuracy needed to fully reconstruct the continuous energy sensitivity profile, however this comes at the expense of drastically increasing the run time in order to achieve reasonable statistical convergence.

4.3.2 Treatment of temperature effects

Another issue with the present sensitivity methods is the use of the cross section covariance matrix, this matrix is dependant on the energy group structure, and temperature. The cross section covariance matrix is obtained from the resonance parameter covariance matrix by the following relation:

$$C_{\sigma\sigma} = \frac{\partial \sigma}{\partial \Gamma} C_{\Gamma\Gamma} \frac{\partial \sigma}{\partial \Gamma}^T \tag{103}$$

The resonance parameter covariance matrix, $C_{\Gamma\Gamma}$ is independent of temperature and energy group structure, however this is not the case for the derivatives $\frac{\partial \sigma}{\partial \Gamma}$. The derivatives must be Doppler Broadened to an appropriate temperature, but the choice of such temperature is not obvious. In a system that contains multiple temperatures, the cross section covariance matrix can only be obtained for a single temperature, this leads to the unfortunate situation where the sensitivities, which correctly account for the temperature, are sandwiched with the covariance matrix, which is oblivious to the multiple temperatures.

4.3.3 Similar Works

As far as the authors are aware, only one study of the direct propagation of resonance parameter uncertainties has ever been done. This work was done by B. Morillon in 2000.

In that work, the neutron flux is expanded using a second order Taylor expansion with respect to the three resonance parameters that describe a single resonance $(E_\lambda, \Gamma_n, \Gamma_\gamma)$ giving the following expression:

$$\begin{aligned}\Delta\psi(\mathbf{r}, \mathbf{\Omega}, E) = \frac{\partial \psi}{\partial E_\lambda}\Delta E_\lambda + \frac{\partial \psi}{\partial \Gamma_n}\Delta\Gamma_n + \frac{\partial \psi}{\partial \Gamma_\gamma}\Delta\Gamma_\gamma \\ + \frac{1}{2}\left(\frac{\partial^2 \psi}{\partial E_\lambda^2}\Delta E_\lambda^2 + \frac{\partial^2 \psi}{\partial \Gamma_n^2}\Delta\Gamma_n^2 + \frac{\partial^2 \psi}{\partial \Gamma_\gamma^2}\Delta\Gamma_\gamma^2 \right) \\ + \frac{\partial^2 \psi}{\partial E_\lambda \partial \Gamma_n}\Delta E_\lambda \Delta\Gamma_n + \frac{\partial^2 \psi}{\partial E_\lambda \partial \Gamma_\gamma}\Delta E_\lambda \Delta\Gamma_\gamma + \frac{\partial^2 \psi}{\partial \Gamma_\gamma \partial \Gamma_n}\Delta\Gamma_\gamma \Delta\Gamma_n \end{aligned} \tag{104}$$

The authors then show that the derivatives of the flux can be expressed with the logarithmic derivatives of the transport and collision kernels, which in turn can be expressed using the derivatives of the cross section.

This methodology is also able to treat the temperature effects by using the SIGMA1 procedure [30] to Doppler broaden the derivative of the cross section with respect to the resonance parameters.

There are two drawbacks of this method. First, it the calculation of 9 derivatives for each resonance, hence this method does not scale well for larger problems. The other drawback is that the method only considers the elastic scattering reaction. The methodology presented in our work is capable of treating all reaction types, including fission.

4.4 Theoretical Derivation

By beginning with he canonical form of the first order perturbation equation, shown below

$$S_{k,x} = \frac{\delta k/k}{\delta x/x} = x\frac{< \phi^\dagger(\lambda\frac{\delta F}{\delta x} - \frac{\delta L}{\delta x})\phi >}{< \phi^\dagger \lambda F \phi >} \tag{105}$$

We will study the special case where the parameter of interest x is the set of parameters describing the multipole formalism. As a matter of nomenclature, we will denote the set of multipole parameters as $\boldsymbol{\pi}$. Here, the bold symbol is used to denote that $\boldsymbol{\pi}$ is really a vector of parameters.

For this case, equation (105) is expressed as:

$$S_{k,\boldsymbol{\pi}} = \frac{\delta k/k}{\delta \boldsymbol{\pi}/\boldsymbol{\pi}} = \boldsymbol{\pi}\frac{< \phi^\dagger(\lambda\frac{\delta F}{\delta \boldsymbol{\pi}} - \frac{\delta L}{\delta \boldsymbol{\pi}})\phi >}{< \phi^\dagger \lambda F \phi >} \tag{106}$$

Where $\phi^\dagger$ is the solution to the adjoint transport equation, and F and L are the fission and loss operators, respectively, in the transport equation. Clearly, evaluating the above expression requires the knowledge of the adjoint flux, as well as the ratio of perturbed operators to perturbed parameters $\frac{\delta L}{\delta \boldsymbol{\pi}}$ and $\frac{\delta F}{\delta \boldsymbol{\pi}}$. In the limit of small perturbations, the ratios converge to first derivative of the operator with respect to the parameter.

Since the fission operator is defined as

$$F\phi = \frac{\chi(r,E)}{4\pi}\int_{4\pi} d\Omega' \int_0^\infty dE' \nu\Sigma_f(r,E')\phi(r,E',\Omega') \tag{107}$$

The only term that has a dependence on the multipole parameters is the fission cross section. Therefore the derivative of the fission operator is

$$\frac{\partial F}{\partial \boldsymbol{\pi}}\phi = \frac{\chi(r,E)}{4\pi}\int_{4\pi} d\Omega' \int_0^\infty dE' \nu\frac{\partial \Sigma_f}{\partial \boldsymbol{\pi}}(r,E')\phi(r,E',\Omega') \tag{108}$$

The loss operator is defined as:

$$L\phi = \Omega\nabla\phi(r,E,\Omega) + \Sigma_t(r,E)\phi(r,E,\Omega) - \int_{4\pi} d\Omega' \int_0^\infty dE' \Sigma_s(r,E'\rightarrow E,\Omega'\rightarrow\Omega)\phi(r,E',\Omega') \tag{109}$$

Taking the derivative with respect to the multipole parameters, we are left with

$$\frac{\partial L}{\partial \boldsymbol{\pi}}\phi = \frac{\partial \Sigma_t}{\partial \boldsymbol{\pi}}(r,E)\phi(r,E,\Omega) - \int_{4\pi} d\Omega' \int_0^\infty dE' \frac{\partial \Sigma_s}{\partial \boldsymbol{\pi}}(r,E'\rightarrow E,\Omega'\rightarrow\Omega)\phi(r,E',\Omega') \tag{110}$$

Therefore, the numerator in equation (106) can be expressed as

$$\begin{aligned}
< \phi^\dagger(\lambda\frac{\delta F}{\delta \boldsymbol{\pi}} - \frac{\delta L}{\delta \boldsymbol{\pi}})\phi > = & \\
& \lambda\int_V dr \int_{4\pi} d\Omega \int_0^\infty dE \phi^\dagger(r,E,\Omega)\frac{\chi(r,E)}{4\pi}\left(\int_{4\pi} d\Omega' \int_0^\infty dE' \nu\frac{\partial \Sigma_f}{\partial \boldsymbol{\pi}}(r,E')\phi(r,E',\Omega')\right) \\
& \qquad - \int_V dr \int_{4\pi} d\Omega \int_0^\infty dE \phi^\dagger(r,E,\Omega)\frac{\partial \Sigma_t}{\partial \boldsymbol{\pi}}(r,E)\phi(r,E,\Omega) \\
& + \int_V dr \int_{4\pi} d\Omega \int_{4\pi} d\Omega' \int_0^\infty dE \int_0^\infty dE' \phi^\dagger(r,E,\Omega)\frac{\partial \Sigma_s}{\partial \boldsymbol{\pi}}(r,E'\rightarrow E,\Omega'\rightarrow\Omega)\phi(r,E',\Omega') \\
& \qquad \equiv S_{fission} + S_{total} + S_{scatter}
\end{aligned} \tag{111}$$

For clarity, the individual terms are defined below

$$S_{fission} \equiv \lambda \int_V dr \int_{4\pi} d\Omega \int_{4\pi} d\Omega' \int_0^\infty dE \int_0^\infty dE' \phi^\dagger(r, E, \Omega) \frac{\chi(r, E)}{4\pi} \nu \frac{\partial \Sigma_f}{\partial \boldsymbol{\pi}}(r, E', \Omega') \phi(r, E', \Omega') \tag{112}$$

$$S_{total} \equiv -\int_V dr \int_{4\pi} d\Omega \int_0^\infty dE \phi^\dagger(r, E, \Omega) \frac{\partial \Sigma_t}{\partial \boldsymbol{\pi}}(r, E) \phi(r, E, \Omega) \tag{113}$$

$$S_{scatter} \equiv \int_V dr \int_{4\pi} d\Omega \int_{4\pi} d\Omega' \int_0^\infty dE \int_0^\infty dE' \phi^\dagger(r, E, \Omega) \frac{\partial \Sigma_s}{\partial \boldsymbol{\pi}}(r, E' \to E, \Omega' \to \Omega) \phi(r, E', \Omega') \tag{114}$$

It is important to note a few things. With S_{total}, the flux and the adjoint are taken at the same phase space location, whereas for $S_{scatter}$ the flux is taken pre-collision and the adjoint is taken post-collision, and for $S_{fission}$ the flux is taken pre-fission, and the adjoint is related to the neutrons born from the fission event.

4.5 Implementation

The implementation used in this work is based on the Iterated Fission Probability (IFP) method for estimating the adjoint flux. In short, IFP estimates the adjoint flux of a neutron in a phase space location p as the total number of fission neutrons produced by the descendants of the original neutron, some number of generations later. In practice, this results in the active cycles in the monte carlo run to be split into three categories; original, latent, and asymptotic. In the original generations, each neutron is given a unique identifier, and all the estimators are tallied. The neutron identifier is passed on from generation to generation through the latent cycles until arriving at the asymptotic generation. It is at the asymptotic generation that the total number of neutrons with the same identifier are tallied, giving an estimate of the adjoint flux for the neutron from the original generation.

$$\phi^\dagger(r, E) = \sum_n \sum_s w_s \nu \Sigma_f l_s \tag{115}$$

Where n is the set of neutrons in the asymptotic generation, and s is the set of paths traveled by those neutrons in the asympototic generation.

Tallying S_{total} is straightforward, it is a tracklength tally.

$$Score\ for\ S_{total} = -\frac{\partial \Sigma_t(r, E)}{\partial \boldsymbol{\pi}} \phi(r, E) \phi^\dagger(r, E) = -\frac{\partial \Sigma_t(r, E)}{\partial \boldsymbol{\pi}} w_s l_s \phi^\dagger(r, E) \tag{116}$$

Here, everything other than the $\phi^\dagger$ term is tallied in the original generation. The $S_{scatter}$ and $S_{fission}$ terms cannot be calculated using a tracklength tally and must therefore use a collision estimator. So at every scattering event, we tally:

$$Score\ for\ S_{scatter} = \frac{\partial \Sigma_s(r, E)}{\partial \boldsymbol{\pi}} \frac{1}{\Sigma_s(r, E)} \phi^\dagger(r, E) \tag{117}$$

and at every fission, we tally:

$$Score\ for\ S_{fission} = \frac{\partial \Sigma_f(r, E)}{\partial \boldsymbol{\pi}} \frac{1}{\Sigma_f(r, E)} \phi^\dagger(r, E) \tag{118}$$

4.6 Results and Validation

The sensitivity of the eigenvalue to the parameters from the first s-wave resonances in U238 were calculated for the pincell problem. The results of the sensitivity calculation were compared against a direct perturbation study.

4.6.1 Pincell

The pincell is a standard PWR fuel pin with 3% enriched UO_2 fuel. The pellet has a radius of 0.39 cm, a gap thickness of 0.01 cm, and a Zirconium clad with a thickness of 0.06 cm. The pitch is 1.26 cm. We simulate the problem with 10,000 neutrons in 7000 active cycles and 20 inactive cycles. The IFP calculation required 3 latent generations.

The sensitivity of the eigenvalue to the first s-wave resonance parameters is summarized in the table below. The eigenvalue is most sensitive to the real and imaginary part of the pole, which roughly correspond to the resonance location, and width, respectively. The eigenvalue was also sensitive to the real part of the absorption residue, which is in a way related to the peak of the resonance.

U^{238} **6.67 eV Resonance**	**Sensitivity** $\frac{\partial k/k}{\partial \pi/\pi}$
$\Re p$	$5.79 \times 10^{-2} \pm 4.78 \times 10^{-3}$
$\Im p$	$-2.35 \times 10^{-2} \pm 3.33 \times 10^{-5}$
$\Re r_{total}$	$3.05 \times 10^{-3} \pm 1.68 \times 10^{-4}$
$\Im r_{total}$	$6.15 \times 10^{-5} \pm 3.69 \times 10^{-6}$
$\Re r_{absorption}$	$-2.81 \times 10^{-2} \pm 1.30 \times 10^{-4}$
$\Im r_{absorption}$	$-5.23 \times 10^{-9} \pm 3.57 \times 10^{-11}$
$\Re r_{fission}$	$1.83 \times 10^{-8} \pm 1.32 \times 10^{-8}$
$\Im r_{fission}$	$4.83 \times 10^{-8} \pm 3.77 \times 10^{-8}$

To test this result, the eigenvalue was calculated as $k = 1.16216$ for the reference state, and a perturbed state was created where the real part of the 6.67 eV pole was increased by 3%. For the perturbed state, the eigenvalue was found to be $k' = 1.16428$. Therefore

$$\frac{\partial k/k}{\partial \pi/\pi} \approx \frac{\frac{k'-k}{k}}{0.03} = 0.0608 \tag{119}$$

This is close to the value we calculated for the sensitivity (0.058), and well within the uncertainty bounds.

U^{238} **20.87 eV Resonance**	**Sensitivity** $\frac{\partial k/k}{\partial \pi/\pi}$
$\Re p$	$2.14 \times 10^{-2} \pm 1.09 \times 10^{-2}$
$\Im p$	$-1.13 \times 10^{-2} \pm 6.34 \times 10^{-5}$
$\Re r_{total}$	$1.93 \times 10^{-3} \pm 8.75 \times 10^{-5}$
$\Im r_{total}$	$1.88 \times 10^{-4} \pm 1.47 \times 10^{-5}$
$\Re r_{absorption}$	$-1.52 \times 10^{-2} \pm 1.04 \times 10^{-4}$
$\Im r_{absorption}$	$-5.42 \times 10^{-9} \pm 7.04 \times 10^{-11}$
$\Re r_{fission}$	$1.58 \times 10^{-7} \pm 9.61 \times 10^{-8}$
$\Im r_{fission}$	$-1.28 \times 10^{-10} \pm 2.44 \times 10^{-9}$

We test this result in a similar manner. A perturbed state was created where the real part of the 20.87 eV pole was increased by 3%. For the perturbed state, the eigenvalue was found to be $k' = 1.16352$. Therefore

$$\frac{\partial k/k}{\partial \pi/\pi} \approx \frac{\frac{k'-k}{k}}{0.03} = 0.0309 \tag{120}$$

This is close to the value we calculated for the sensitivity (0.0214), and within the uncertainty bounds, which are larger for this case than in the previous case.

4.6.2 Temperature Effects

One of the major improvements that this capability offers over existing methods is the ability to fully take into account the temperature effects. To demonstrate this, we look at the pincell problem once again, and we calculate the sensitivity to the first s-wave resonance of U238 at three different fuel temperatures. We compare the sensitivities and show that temperature effects do matter.

$\mathbf{U^{238}}$ **6.67eV**	**Sensitivity** $\frac{\partial k/k}{\partial \pi/\pi}$		
Temperature	0K	600K	1200K
k_{eff}	1.194	1.149	1.133
$\Im p$	$\mathbf{-2.44 \times 10^{-2} \pm 4.95 \times 10^{-5}}$	$-2.27 \times 10^{-2} \pm 3.95 \times 10^{-5}$	$-2.13 \times 10^{-2} \pm 3.62 \times 10^{-5}$
$\Re r_{total}$	$2.62 \times 10^{-3} \pm 3.42 \times 10^{-4}$	$3.87 \times 10^{-3} \pm 1.74 \times 10^{-4}$	$\mathbf{5.00 \times 10^{-3} \pm 1.63 \times 10^{-4}}$
$\Re r_{absorption}$	$-2.79 \times 10^{-2} \pm 3.73 \times 10^{-4}$	$-2.75 \times 10^{-2} \pm 1.90 \times 10^{-4}$	$-2.76 \times 10^{-2} \pm 1.74 \times 10^{-4}$

The results table shows three separate parameters that illustrate the importance of the temperature effects. The parameter in bold is the most significant sensitivity. It is clear to see that for the case of the Imaginary part of the pole, the sensitivity is most significant at lower temperatures. In contrast, the real part of the total residue is most significant at the higher temperature. Finally, for the real part of the absorption residue, temperature effects seem to not matter at all. This shows that temperature effects can be significant, and they do bias the results, however the direction of the bias is not predictable. This motivates the need to explicitly account for temperature in sensitivity calculations.

4.7 Conclusion and Future Work

In this work, we have developed a method to calculate the sensitivities of the eigenvalue in monte carlo simulation to the underlying nuclear data parameters. We have shown that the results are accurate up to small perturbations in the nuclear data parameters.

In order to calculate the uncertainty in the eigenvalue from the sensitivities, we need to use a covariance matrix. Future work will look at ways to convert a resonance parameter covariance matrix, which is obtained in file 32 in ENDF, to a multipole parameter covariance matrix.

Currently this method uses IFP to calculate the adjoint, this can be quite memory intensive. The state-of-the-art method for adjoint weighted tallies is the CLUTCH method developed by Perfetti et al [**?**]. A variant of the CLUTCH method has been implementing in OpenMC by Peng [**?**]. Future work will look at replacing IFP in this method with CLUTCH.

Finally, future work will look at obtaining sensitivities to general responses. Examples of such general responses include fission-to-capture ratio and power peaking factors.

5 Multipole Covariance Matrix

The purpose of this section is to describe the efforts made to convert the Resonance Parameters Covariance Matrix (ENDF File 32 [7]) to the Multipole Covariance matrix. The conversion is needed in order to use the proposed methods that rely on a pole and residue cross section definition. Two approaches have been developed and tested and details are provided below following a description of the data and tools used in this work.

5.1 Tools

This section describes the tools used in the conversion process, as well as the efforts to incorporate the tools within OpenMC's python API. This total integration has vastly improved the work flow of the conversion process.

5.1.1 ENDF Library

As a starting point, the ENDF library contains all the data that we need to perform the conversion task. File 2 contains all the information on the resonance parameters, and File 32 contains the associated resonance parameter covariance.

Table 2: Isotopes in the ENDF 7.1 Library containing covariance data (File 32)

Isotope			
Na-23	Ni-58	Tl-203	Cm-243
Cl-35	Ni-60	Tl-205	Cm-244
K-39	Gd-152	Th-228	Cm-245
K-41	Gd-153	Th-229	Cm-246
Ti-46	Gd-154	Th-230	Cm-247
Ti-47	Gd-155	Th-232	Cm-248
Ti-48	Gd-157	Pa-232	Bk-249
Ti-49	Gd-160	U-232	Cf-249
Ti-50	Tm-169	Np-236	Cf-250
Cr-50	Tm-170	Np-238	Cf-251
Cr-52	W-182	Pu-236	Cf-252
Cr-53	W-183	Pu-244	
Cr-54	W-184	Am-241	
Mn-55	W-186	Cm-242	

However, File 32 is not included for all evaluations. A table containing the isotopes which have File 32 available in the ENDF/B-VII.1 library is included here. While the File 32 data for ^{233}U, ^{235}U, ^{238}U, and ^{239}Pu are not available in the regular distribution due to memory concerns, they can be obtained directly from Oak Ridge National Lab.

5.1.2 OpenMC

The OpenMC code [31], and specifically the OpenMC python API, now has the capability to read an ENDF file, including File 2 and File 32. The python API has been extended to randomly sample from a resonance parameter covariance matrix to create a new instance of the cross section, which is then exported as a HDF5 file for use in OpenMC.

5.1.3 Vector Fitting

Vector Fitting is an algorithm that was developed by the signal processing community that allows one to fit a signal to a rational function [32]. Since in the multipole formalism, the cross section is exactly a rational function in $\sqrt{E}$, a variant of vector fitting was developed at MIT to specifically fit cross sections in the multipole format [2]. This algorithm has been incorporated in the OpenMC python API.

5.1.4 OpenW

OpenW is a code developed at MIT to convert ENDF files to Windowed Multipole [25] files. Specifically, OpenW performs the windowing process to get a windowed multipole file from a multipole file, in other words, OpenW performs the windowing process. This code has also recently been integrated in the python API of OpenMC.

5.2 Conversion Process - Direct Sampling Approach: The Titanium Case

This section will describe the details of the conversion process through direct sampling. The process is quite simple: use the resonance parameter covariance matrix to sample many independent sets of resonance parameters, convert the resonance parameters to windowed multipole, and finally, use the converted independent sets of multipoles to construct a multipole covariance matrix.

The isotope Ti-46 has been used to test the conversion process. Ti-46 was chosen because it is the smallest isotope that both includes File 32 in the evaluation and is included in the OpenMC windowed multipole library.

5.2.1 Sampling from file 32

Using a modified OpenMC API, the Ti-46 resonance parameters were sampled to produce 1000 independent sets of resonance parameters. Each of these sets was exported to an hdf5 file.

The hdf5 file only contains the resonance parameters. For the purpose of this process, the background cross section (File 3) has been set to zero.

5.2.2 Sampling negative parameters

One of the issues with using File 32, is that the assumption that the parameters are distributed normally results in a non-negligible probability of sampling a negative resonance parameter. These negative parameters cannot be discarded without affecting the mean of the parameters. Currently the negative parameters are kept because they can still be converted to multipoles without any problems, however it is hard to argue that the parameters are physical, and therefore this topic will need to be studied further.

Previous attempts at using the resonance parameter uncertainties to quantify uncertainties in nuclear calculations have avoided the issue of sampling negative cross sections from file 32 altogether. Worthy of note is the approach of Rochman and Koning [14, 3] with TALYS. Their approach samples the resonance parameters independently, i.e. assuming no correlations between parameters, and accept or reject the samples based on whether the resulting cross sections fall within experimental uncertainties.

One possible solution could be to consider the parameters as distributed log-normally as opposed to normally. This eliminates the possibility of sampling a negative parameter. The procedure of sampling a log normal distribution will be evaluated further in the near future.

As a reminder, if $\mathbf{X} \sim \mathcal{N}(\boldsymbol{\mu}, \boldsymbol{\Sigma})$ is a multivariate normal distribution then $\mathbf{Y} = \exp(\mathbf{X})$ has a multivariate log-normal distribution with mean

$$\mathrm{E}[\mathbf{Y}]_i = e^{\mu_i + \frac{1}{2}\Sigma_{ii}} \tag{121}$$

and covariance matrix

$$\mathrm{Var}[\mathbf{Y}]_{ij} = e^{\mu_i + \mu_j + \frac{1}{2}(\Sigma_{ii} + \Sigma_{jj})}(e^{\Sigma_{ij}} - 1) \tag{122}$$

5.2.3 Converting to Windowed Multipole

The 1000 independent samples were converted to the windowed multipole format. The size of the inner window, and the fit order, were determined by using the same settings that generated the windowed multipole file included in the OpenMC library.

5.2.4 What's in a Windowed Multipole file?

The windowed multipole file contains all the data necessary to reconstruct the cross section. The file reports the formalism of the ENDF file, which is either Multi Level Breit-Wigner or Reich-Moore. The file contains information on the windows, data such as index of the first and last poles in each window, and the coefficients of the curve fit. Each pole is reported with its residues. The following table describes the pole parameters.

Table 3: The parameters that describe each pole

Formalism	Parameter	Description
Multi Level Breit-Wigner	p	pole
	r_t	total residue
	r_{comp}	competitive residue
	r_{abs}	absorption residue
	r_{fis}	fission residue
Reich-Moore	p	pole
	r_t	total residue
	r_{abs}	absorption residue
	r_{fis}	fission residue height

5.2.5 Analysis of the converted files

Out of the 1000 sampled sets of resonance parameters, 859 provided a solution with the expected number of poles (i.e. 108 poles). The remaining simulations either failed to meet some of the accuracy requirements of the windowed multipole processing or simply created a non-physical number of poles. For analysis purposes,

we discarded these samples but additional work would be needed to determine the cause of the failure and that no bias is introduced in discarding them.

A final check that was also performed on the windowed multipole files to see if the processed cross sections were strictly positive in the resonance region. To analyze this, the (n, γ) cross section was reconstructed on a very fine energy grid, and the files that result in a negative cross section were recorded. After this analysis, only 12 evaluations resulted in a cross section that was always positive. It should be noted that this is also expected when sampling from the original resonance parameter space. This result casts serious doubt on the value and quality of the covariance data provided with the evaluation. If the data was in any way accurate, it should not produce negative cross sections under any circumstance, let alone over 98% of the time.

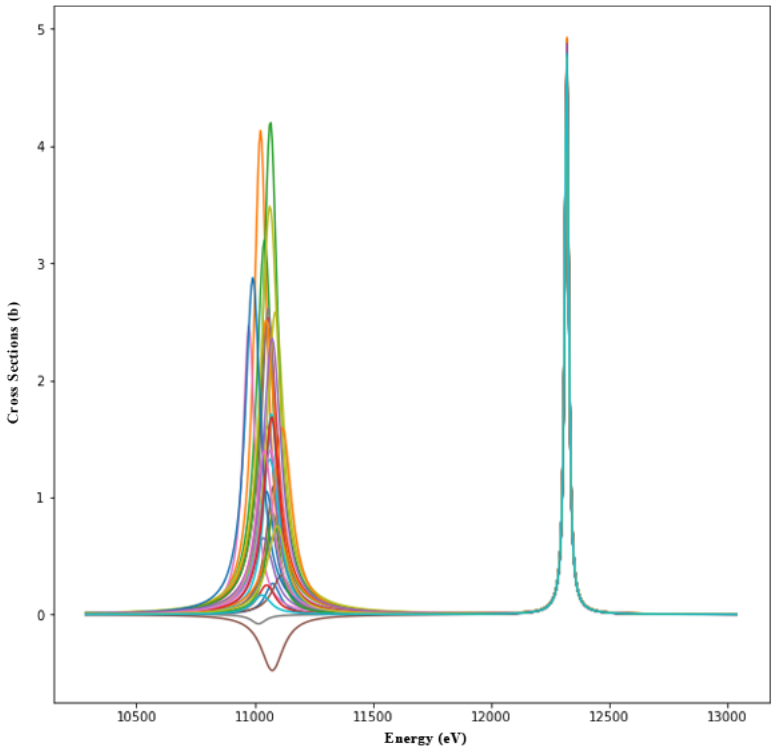

Figure 14: The (n, γ) cross section for 30 randomly selected instances in a small energy range. Note how some of the cross sections become negative. Also note how the first resonance has a much higher uncertainty than the second resonance

Admittedly, part of the reason we are seeing negative cross sections is a fault of the Multi Level Breit-Wigner (MLBW) formalism, which is the formalism of the Ti-46 evaluation. The MLBW equations do not guarantee a positive cross section, unlike the equations that describe the Reich-Moore formalism. Future work will verify this by processing nuclides in the Reich-Moore formalism.

Since 12 is not a statistically significant sample size, and since we cannot discard the negative cross sections without seriously affecting the Gaussian sampling, it was decided to use 859 windowed multipole files that resulted in the exact number of poles (i.e. 108) for the purposes of calculating and testing a multipole covariance matrix.

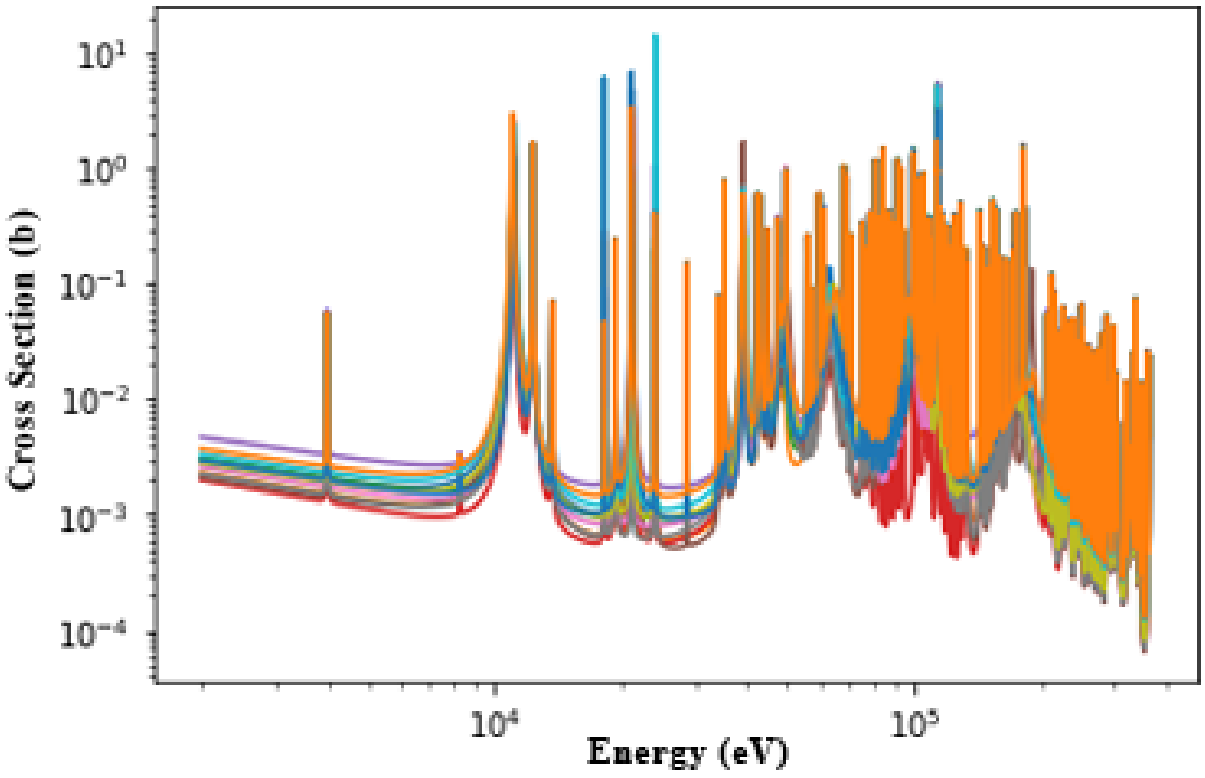

Figure 15: The (n, γ) cross section for the 12 instances of Ti-46 that result in a strictly positive cross section

5.3 Conversion Process - Direct Sampling Approach: The Gadolinium Case

A lot of the issues that were faced in converting Titanium were due to negative cross sections. We postulated that if we study an evaluation using Reich-Moore, we should never see negative cross sections, and therefore, we can safely perform the conversion. In order to test this, we attempted to convert the covariance matrix of Gd-157 in figure 16.

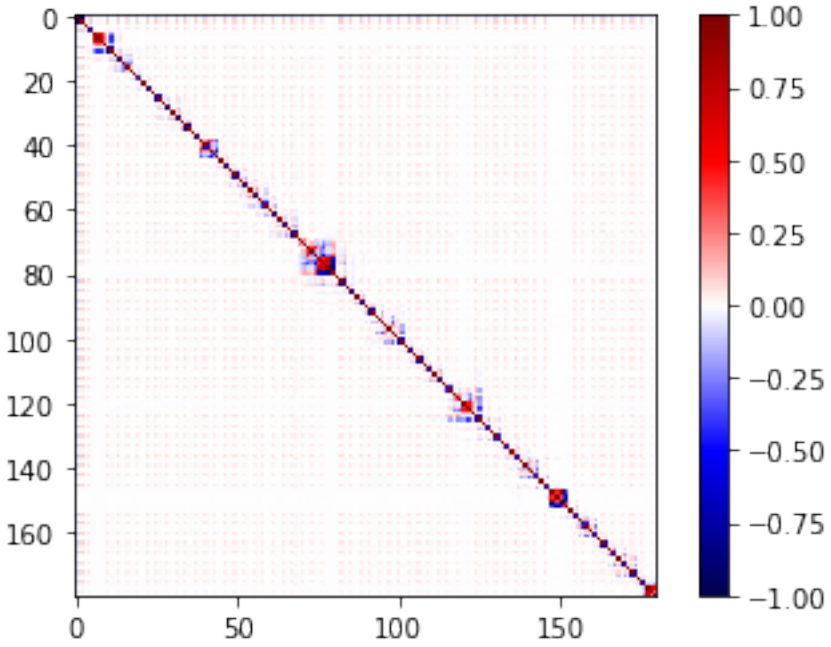

Figure 16: Gd-157 Correlation matrix from file 32

5.3.1 Linearity of the Cross Section

One of the fundamental assumptions made is that everything is linear. This means that the resonance parameters are distributed linearly, and therefore the cross section is also distributed linearly. To test this assumption we sampled 2000 different sets of resonance parameters, and then reconstructed the cross sections. We then generate a histogram of the cross section at a specific energy, we chose an arbitrary energy $E = 0.1eV$ and the results are shown in figure 17. Note that it appears that the histogram does deviate from a gaussian, and that a normal distribution does not perfectly capture the variation in the cross section.

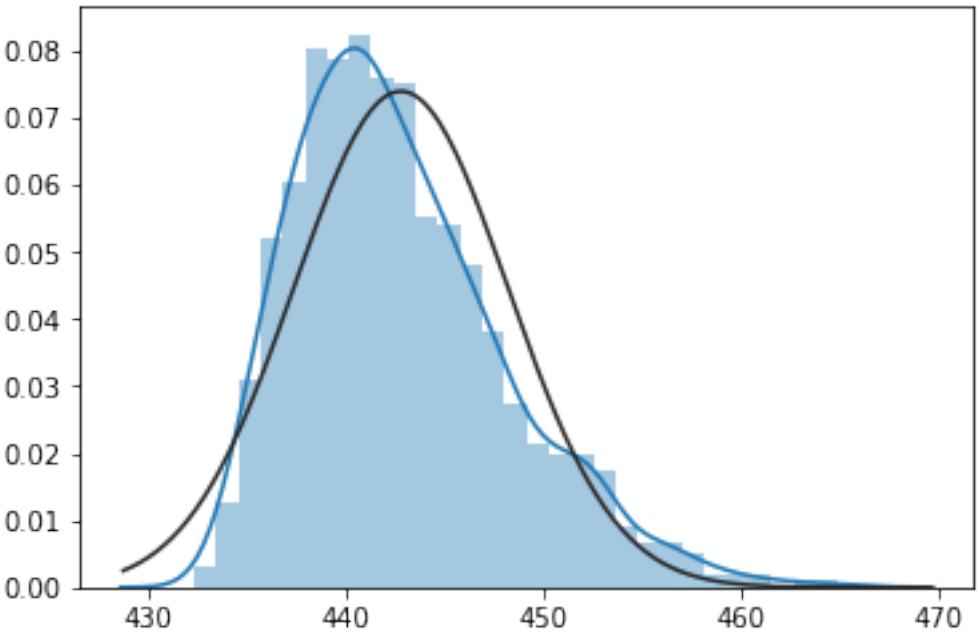

Figure 17: Histogram of the cross section at $E = 0.1eV$, with a gaussian fit overlaid

5.3.2 Evaluating the accuracy of the multipole covariance matrix

We expect that it shouldn't matter if we use a multipole covariance matrix, or a resonance parameter covariance matrix to sample new cross sections. In other words, we expect the distribution of cross sections from both covariance matrices to be identical. This gives us a way to test the accuracy of our conversion. Figure 18 shows a set of 10 cross sections sampled from the estimated multipole covariance matrix. We can already see that the distribution of cross sections is very different from the one obtained via file 32. To drive this point home, the gaussian fit of the cross section histogram at $E = 0.1eV$ is plotting for both the file 32 samples and the multipole samples, and it is clear that the distributions do not match in figure 19. Specifically, it is worth noting that the there is a slight difference in the mean of the two distributions, but a massive difference in the variance.

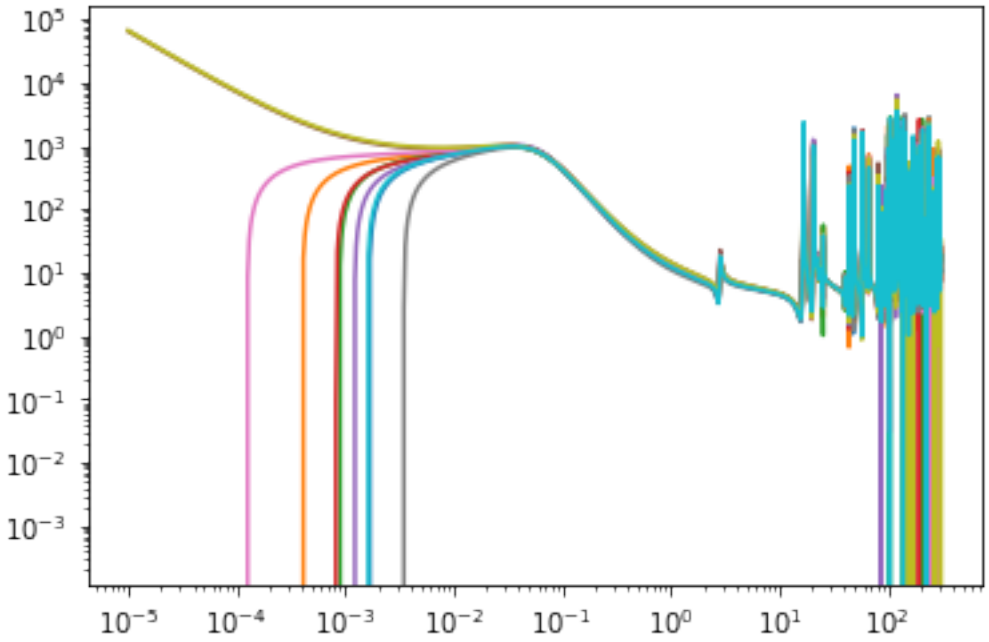

Figure 18: cross sections sampled from the multipole covariance matrix

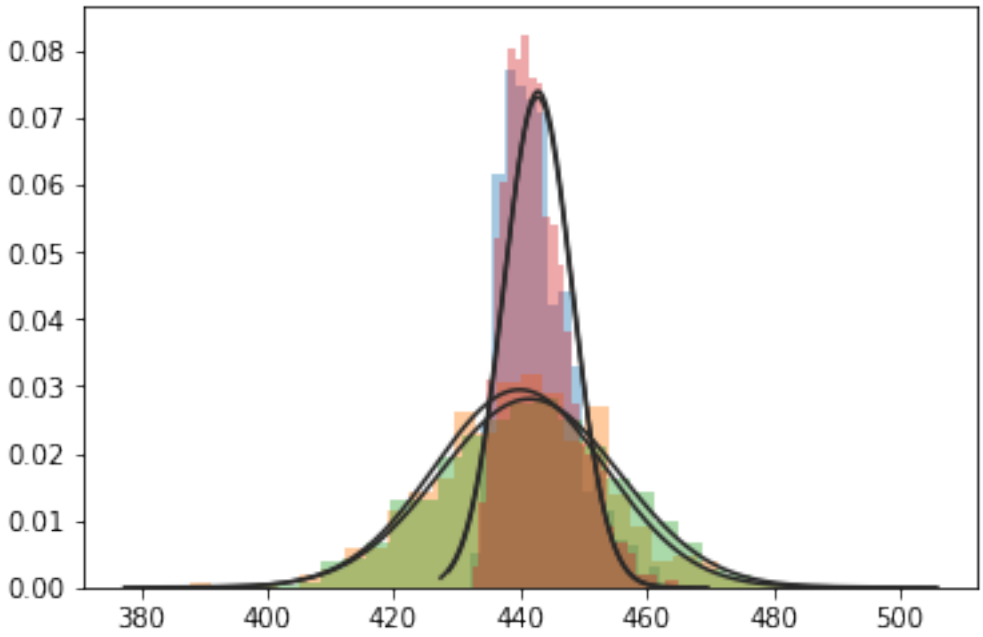

Figure 19: Gaussian fit of the file 32 cross sections and multipole cross sections

5.4 Resonance Ordering

One of the first things that we notice when looking at the windowed multipole files is that the ordering of the poles is inconsistent between files. The poles need to be put into the same, consistent ordering across samples for the covariance matrix to be constructed. The difficulty being that the way to reorder the poles is not clear as each pole does not have a unique identifier.

ENDF files sort the resonances first by spin group (s-wave, p-wave, etc.), and then by the position of the resonance E_λ. OpenW on the other hand, sorts the poles just by the real part of the pole position, which correlates to the position of the resonance. For small perturbations in resonance parameters, this does not pose an issue, however in some cases, we see that the uncertainty in some of the resonances are large enough that for some samples, these resonances "jump over" other resonances.

5.5 Future work in conversion

Currently, we have only looked at a naive estimator of the covariance. That is, given a set of samples $X = \{X_1, X_2, ..., X_n\}$, the covariance can be estimated using:

$$C = E[(X - E(X))(X - E(X))^T] \tag{123}$$

This is an unbiased estimator, and in the limit of $n \to \infty$, converges to the true covariance matrix. However, this estimator has a high variance when the number of samples n is less than, or equal to the dimension of the sample d. In our case, the dimension of the sample is the number of resonance parameters, which is on the order of a few thousand. This means that the estimator used is not necessarily the best choice. Another way to think about it is that the covariance matrix we are trying to estimate is of size $d \times d$, and we are trying to estimate it with $n \times d$ samples. One way to get around it is to impose a certain structure on the covariance matrix, that is to band the matrix in such a way that values appearing far from the diagonal are penalized. While this may not be the best approach for our case, it hints at a possible way forward. It is possible to impose a structure for the matrix based on the physics to develop new estimators, for example, we should not expect resonances in different spin groups to be correlated. Development of new estimators is a topic of current work. Windowing, in effect, is also another way of imposing a certain structure on the covariance matrix. Looking at the covariance of windowed files is also a topic of current work.

5.6 Conversion Process - Numerical Derivative Approach

The direct sampling approach is quite straightforward, but it has the major disadvantage of not being able to guarantee cross sections that are always positive. It was therefore necessary to explore a different approach.

One such approach is to use the chain rule to expand the multipole covariance matrix in terms of the resonance parameter covariance matrix.

$$C_\pi = \frac{\partial \pi}{\partial \Gamma} C_\Gamma \frac{\partial \pi}{\partial \Gamma}^T \tag{124}$$

where C_π is the multipole covariance matrix, C_Γ is the resonance parameter covariance matrix, and $\frac{\partial \pi}{\partial \Gamma}$ is the jacobian matrix with derivatives of multipole parameters with respect to resonance parameters. This jacobian matrix could be estimated numerically by systematically introducing a small perturbation to each resonance parameter in the original ENDF evaluation, converting the perturbed ENDF file to a WMP file, and comparing that file to the reference WMP file to calculate the derivative. Each perturbation of a resonance parameter yields a column of the jacobian matrix, doing this for each resonance parameter will yield the full matrix.

The main advantage of this method is that by only perturbing the resonance parameter by a very small amount, the issue of negative cross sections, and misordering of the poles, are completely eliminated. This approach was validated on a small fictional covariance matrix by comparing the converted matrix obtained via the numerical derivative approach and the matrix obtained via the direct sampling approach and showing that they converge. The drawback of this method is that it assumes that the conversion process can be approximated by a linear expansion. This assumption is valid for the case of small perturbations in the resonance parameters, however we have seen that the perturbations can be quite large. The accuracy of this method can be assessed by calculating higher order derivatives and observing how the results change.

5.7 Results from Ti-46 Conversion

The Ti-46 resonance parameter covariance matrix was converted to a multipole parameter covariance matrix using the Monte Carlo methodology. The covariance matrix is dominated by the variance of a few of the resonance parameters, therefore to better see the structure of the matrix, the correlation matrix is plotted in figure 20. Note that the matrix is not sparse, however the strongest correlations exist on or near the diagonal. This implies that resonances close in energy are heavily correlated.

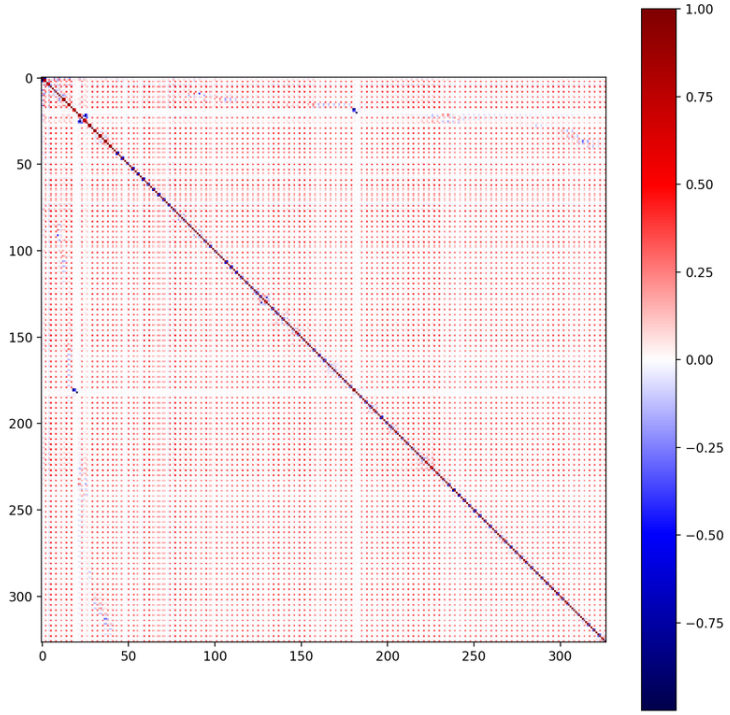

Figure 20: Ti-46 Correlation matrix taken directly from File 32

The converted multipole correlation matrix in figure 21 shares many characteristics with the resonance parameter correlation matrix. Both are full matrices with dominant terms near the diagonal. It is also worth noticing that the multipole correlation matrix is more than quadruple the size of the resonance parameter correlation matrix. This is because in the R-Matrix formalism, the resonance is described by 4 real parameters $(E_\lambda, \Gamma_f, \Gamma_n, \Gamma_\gamma)$, but since Ti-46 is not fissionable, the fission width is excluded from the file 32 correlation matrix, whereas in the multipole formalism, each pole is described by 5 complex parameters $(p, r_t, r_{comp}, r_{abs}, r_{fis})$ where again the fission residue was not included. In creating the multipole covariance matrix, the real and imaginary part of each parameter was treated as a separate real-valued parameter, thereby doubling the number of parameters.

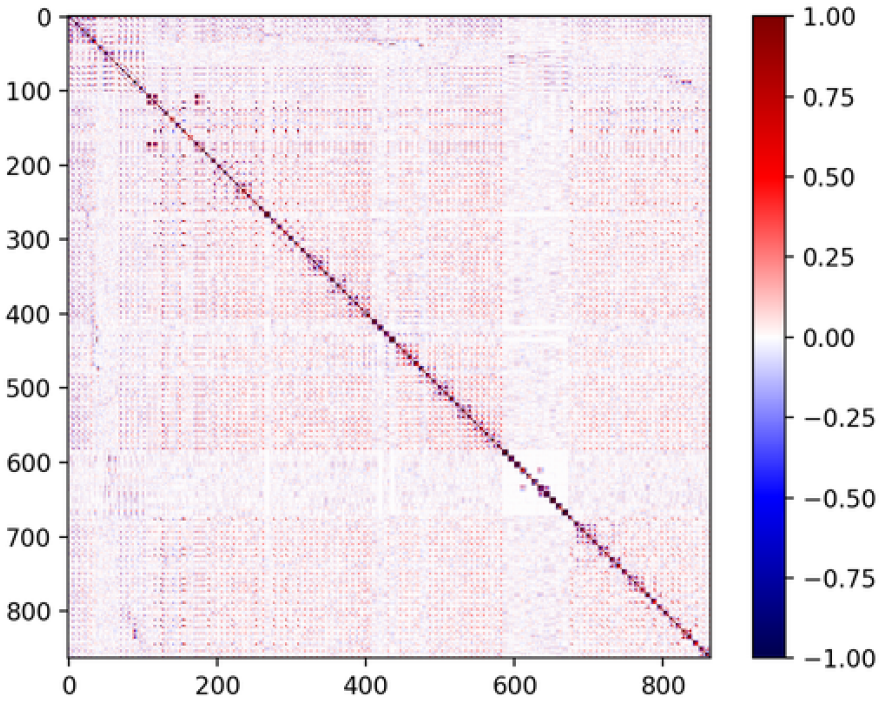

Figure 21: Ti-46 Multipole Correlation matrix converted from File 32

5.8 Analytic contour integrals conversion of resonance parameters covariances to multipole covariances

In order to sample poles and residues that express the uncertainty on the cross section, as expressed in the resonance parameters covariance matrix, one must determine a distribution of poles and residues.

A first-order approach to doing so is to assume that the relation from resonance parameters $\{\Gamma\}$ to poles and residues $\{\pi\}$ is locally linear, which stands for very small deviations from the mean. In that case, the chain rule entails the poles and residues $\{\pi\}$ are also subject to a Gaussian distribution, the covariance of which is given by the so-called sandwich rule (124).

From the latter, the key to obtaining the poles and residues $\{\pi\}$ covariance matrix $\mathrm{Cov}(\pi)$ lies in the sensitivities $\left(\frac{\partial\pi}{\partial\Gamma}\right)$.

We have developed and analytic way to calculate these sensitivities as follows.

Definition 1. Holomorphic and Cartesian complex differentials.
Let $z \in \mathbb{C}$, $z = x + \mathrm{i}y$, $x, y \in \mathbb{R}$. The holomorphic differential is defined as

$$\partial_z \coloneqq \frac{1}{2}\left(\partial_x - \mathrm{i}\partial_y\right) \tag{125}$$

Note that $\partial_z z = 1$, and $\partial_z \overline{z} = 0$, where $\overline{z} \coloneqq x - iy$ designates the complex conjugate.

We here define the Cartesian differential as:

$$\eth_z \coloneqq \partial_x + \mathrm{i}\partial_y \tag{126}$$

Note that $\eth_z z = 0$, and $\eth_z \overline{z} = 2$.

Lemma 1. Windowed Multipole Sensitives
Let $z \in \mathbb{C}$ be the complex, analytically continued square-root-of-energy, so that for real energies above threshold we have $z = \sqrt{E}$, and consider the Windowed Multipole cross section, i.e. locally of the form:

$$\sigma(z) \underset{\mathcal{W}(E)}{=} \sum_{n\geq -2} a_n z^n + \frac{1}{z^2}\Re^{\mathrm{al}}\left[\sum_{j=1}^{N_p}\frac{r_j}{z-p_j}\right] \tag{127}$$

then the cross section sensitivities to multipoles $\frac{\partial\sigma}{\partial\pi}(z)$ (i.e. the partial differentials of the cross section with respect to multipoles) are then given, in window $\mathcal{W}(E)$, by:

$$
\begin{aligned}
\frac{\partial\sigma}{\partial a_n}(z) &= z^n \\
\frac{\partial\sigma}{\partial p_j}(z) &= \frac{1}{z^2}\frac{\frac{r_j}{2}}{(z-p_j)^2} \quad , \quad \frac{\partial\sigma}{\partial p_j^*}(z) = \frac{1}{z^2}\frac{\frac{r_j^*}{2}}{(z-p_j^*)^2} \\
\frac{\eth\sigma}{\eth p_j}(z) &= \frac{1}{z^2}\frac{r_j^*}{(z-p_j^*)^2} \quad , \quad \frac{\eth\sigma}{\eth p_j^*}(z) = \frac{1}{z^2}\frac{r_j}{(z-p_j)^2} \\
\frac{\partial\sigma}{\partial\Re[p_j]}(z) &= \frac{1}{z^2}\Re^{\mathrm{al}}\left[\frac{r_j}{(z-p_j)^2}\right] \quad , \quad \frac{\partial\sigma}{\partial\Im[p_j]}(z) = \frac{1}{z^2}\Re^{\mathrm{al}}\left[\frac{\mathrm{i}\,r_j}{(z-p_j)^2}\right] \\
\frac{\partial\sigma}{\partial r_j}(z) &= \frac{1}{z^2}\frac{\frac{1}{2}}{z-p_j} \quad , \quad \frac{\partial\sigma}{\partial r_j^*}(z) = \frac{1}{z^2}\frac{\frac{1}{2}}{z-p_j^*} \\
\frac{\eth\sigma}{\eth r_j}(z) &= \frac{1}{z^2}\frac{1}{z-p_j^*} \quad , \quad \frac{\eth\sigma}{\eth r_j^*}(z) = \frac{1}{z^2}\frac{1}{z-p_j} \\
\frac{\partial\sigma}{\partial\Re[r_j]}(z) &= \frac{1}{z^2}\Re^{\mathrm{al}}\left[\frac{1}{z-p_j}\right] \quad , \quad \frac{\partial\sigma}{\partial\Im[r_j]}(z) = \frac{1}{z^2}\Re^{\mathrm{al}}\left[\frac{\mathrm{i}}{z-p_j}\right]
\end{aligned}
\tag{128}
$$

Moreover, the cross section sensitivities to resonance parameters $\frac{\partial\sigma}{\partial\Gamma}(z)$ (i.e. the partial differentials of the cross section with respect to resonance parameters) are subject to the following multipole representation:

$$
\frac{\partial\sigma}{\partial\Gamma}(z) \underset{\mathcal{W}(E)}{=} \sum_{n\geq -2}\left(\frac{\partial a_n}{\partial\Gamma}\right)z^n + \frac{1}{z^2}\Re^{\mathrm{al}}\left[\sum_{j=1}^{N_p}\frac{\left(\frac{\partial r_j}{\partial\Gamma}\right)}{z-p_j} + \frac{\left(r_j\cdot\frac{\partial p_j}{\partial\Gamma}\right)}{(z-p_j)^2}\right] \tag{129}
$$

Proof. Sensitivities (128) and (129) are a direct consequence of partial differentiation of the windowed multipole representation (127), by $\frac{\partial\cdot}{\partial\pi}$ and $\frac{\partial\cdot}{\partial\Gamma}$ respectively. □

Having derived the sensitivities, we can now establish the main result of this section: theorem 1, which establishes a means for computing the Windowed Multipole covariances.

Theorem 1. Windowed Multipole Covariances
Let us assume we are provided the analytic continuation (129) of the cross section sensitivities to resonance parameters $\frac{\partial\sigma}{\partial\Gamma}(z)$, then the sensitivities $\left(\frac{\partial\pi}{\partial\Gamma}\right)$ of the multipoles $\{\pi\} \triangleq \{p_j, r_j^{cc'}\}$ with respect to the resonance parameters $\{\Gamma\} \triangleq \{E_\lambda, \gamma_{\lambda,c}\}$ can be obtained from the following contour integrals in the complex plane:

$$
\begin{aligned}
\frac{1}{2}\frac{r_j}{p_j^2}\cdot\left(\frac{\partial p_j}{\partial\Gamma}\right) &= \frac{1}{2\pi\mathrm{i}}\oint_{\mathcal{C}_{p_j}}(z-p_j)\frac{\partial\sigma}{\partial\Gamma}(z)\mathrm{d}z = \frac{\epsilon}{2\pi}\int_{\theta=0}^{2\pi}(p_j+\epsilon\mathrm{e}^{\mathrm{i}\theta})\frac{\partial\sigma}{\partial\Gamma}(p_j+\epsilon\mathrm{e}^{\mathrm{i}\theta})\mathrm{e}^{\mathrm{i}\theta}\mathrm{d}\theta \\
\frac{1}{2}\frac{1}{p_j^2}\cdot\left(\frac{\partial r_j}{\partial\Gamma}\right) - \frac{r_j}{p_j^3}\cdot\left(\frac{\partial p_j}{\partial\Gamma}\right) &= \frac{1}{2\pi\mathrm{i}}\oint_{\mathcal{C}_{p_j}}\frac{\partial\sigma}{\partial\Gamma}(z)\mathrm{d}z = \frac{\epsilon}{2\pi}\int_{\theta=0}^{2\pi}\frac{\partial\sigma}{\partial\Gamma}(p_j+\epsilon\mathrm{e}^{\mathrm{i}\theta})\mathrm{e}^{\mathrm{i}\theta}\mathrm{d}\theta \\
\left(\frac{\partial a_n}{\partial\Gamma}\right) + \delta_{-1,n}\Re^{\mathrm{al}}\left[\sum_{j=1}^{N_p}\frac{2\left(r_j\cdot\frac{\partial p_j}{\partial\Gamma}\right) - p_j\left(\frac{\partial r_j}{\partial\Gamma}\right)}{p_j^3}\right] + \delta_{-2,n}\Re^{\mathrm{al}}&\left[\frac{\left(r_j\cdot\frac{\partial p_j}{\partial\Gamma}\right) - p_j\left(\frac{\partial r_j}{\partial\Gamma}\right)}{p_j^2}\right] \\
&= \frac{1}{2\pi\mathrm{i}}\oint_{\mathcal{C}_0}\frac{1}{z^{n+1}}\frac{\partial\sigma}{\partial\Gamma}(z)\mathrm{d}z = \frac{1}{2\pi}\int_{\theta=0}^{2\pi}\frac{\mathrm{e}^{-\mathrm{i}(n+1)\theta}}{\epsilon^n}\frac{\partial\sigma}{\partial\Gamma}(\epsilon\mathrm{e}^{\mathrm{i}\theta})\mathrm{e}^{\mathrm{i}\theta}\mathrm{d}\theta
\end{aligned}
\tag{130}
$$

To first order, this entails the Windowed Multipole covariance is given by:

$$
\mathrm{Cov}(\pi) = \left(\frac{\partial\pi}{\partial\Gamma}\right)\mathrm{Cov}(\Gamma)\left(\frac{\partial\pi}{\partial\Gamma}\right)^{\dagger} \tag{131}
$$

Proof. We start by performing a partial fraction expansion of (129) yielding:

$$\frac{\partial \sigma}{\partial \Gamma}(z) = \sum_{n \geq -2} \left(\frac{\partial a_n}{\partial \Gamma} \right) z^n + \Re^{\text{al}} \left[\sum_{j=1}^{N_p} \frac{2\left(r_j \cdot \frac{\partial p_j}{\partial \Gamma}\right) - p_j \left(\frac{\partial r_j}{\partial \Gamma}\right)}{p_j^3 z} + \frac{\left(r_j \cdot \frac{\partial p_j}{\partial \Gamma}\right) - p_j \left(\frac{\partial r_j}{\partial \Gamma}\right)}{p_j^2 z^2} + \frac{p_j \left(\frac{\partial r_j}{\partial \Gamma}\right) - 2\left(r_j \cdot \frac{\partial p_j}{\partial \Gamma}\right)}{p_j^3 (z - p_j)} + \frac{\left(r_j \cdot \frac{\partial p_j}{\partial \Gamma}\right)}{p_j^2 (z - p_j)^2} \right]$$

We now invoke Cauchy's Residues Theorem to compute the different residues associates with poles 0 or p_j, multiplying correspondingly by z^n or $(z - p_j)$ when necessary, which yields (130). □

To validate the contour integrals (130), we compared the method to close-form sensitivity functions we derived on the first resonance of U-238, as recorded in Figure 22.

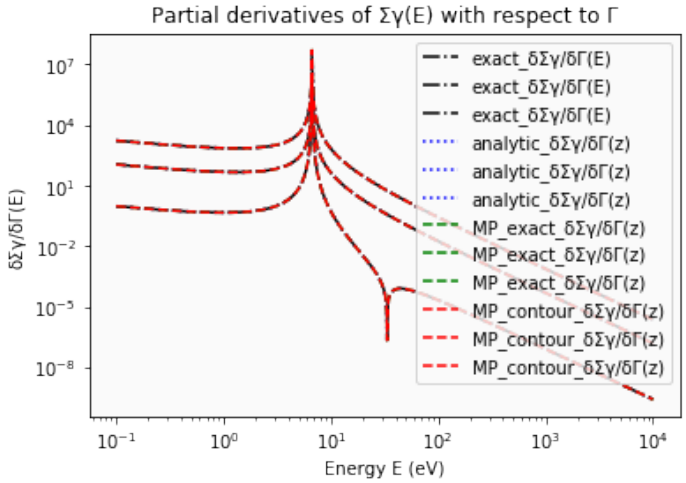

Figure 22: Contour integrals method for Multipole sensitivites validation: the sensitivities to resonance parameters of the first resonance of U-238 were computed explicitly, analytically, and from the contour-integrals method computing the Mutlipole sensitivities from (130) and plotting the sensitivities from (129). All methods yield the same result.

Importantly, contour integrals cannot be performed without having an analytic representation of the partial derivatives of the cross section at complex energies, $\frac{\partial \sigma}{\partial \Gamma}(z)$. This formalism was made possible as a result of the findings drawn from years of research carried out at MIT, Oak Ridge National Laboratory, and Los Alamos National Laboratory investigating the mathematical properties of nuclear cross sections as derived from R-matrix theory [28, 27, 2, 33, 34].

6 Conclusion

This report documents recent progress on many aspects of current research at MIT to quantify the uncertainty of nuclear simulations when using Monte Carlo transport solvers. In particular, we established an analytic benchmark to serve as a tool for validation and verification of subsequent uncertainty quantification methods. This benchmark is also the first time resonance self-shielding is explicitly solved from R-matrix theory of nuclear interactions to the Bolzmann transport equation. Various methods to convert the resonance parameters covariance matrices (ENDF File 32) into a multipole covariance matrix have been explored, and preliminary results on these methods are here documented. Moreover, we explored new approaches to performing the uncertainty quantification in the Monte Carlo simulation, either by re-visiting the sensitivity approach from a windowed multipole lenses, or by proposing a new Embedded Monte Carlo approach,

whereby each neutrons perceives a new possible realization of the physics, given our epistemic uncertainty on nuclear data. All these elements constitute fundamental bricks that, upon assemble, could yield to breakthrough improvement in the uncertainty quantification performance of Monte Carlo reactor physics codes.

References

[1] V. Sobes, P. Ducru, A. Alhajri, B. D. Ganapol, B. Forget, An Analytic Benchmark for the Neutron Boltzmann Transport Downscattering Problem, i. flux & eigenvalue solutions, Computer Physics Communicationswork-in-progress.

[2] X. Peng, P. Ducru, S. Liu, B. Forget, J. Liang, Converting point-wise nuclear cross sections to pole representation using regularized vector fitting, Computer Physics Communications 224 (2018) 52–62.

[3] D. Rochman, W. Zwermann, A. Koning, al., Nuclear data uncertainty propagation: Perturbation vs. monte carlo, Nuclear Science and Engineering 177 (2014) 337–349.

[4] P. Ducru, J. Liang, V. Sobes, A. Alhajri, I. Meyer, B. Forget, K. Smith, EMBEDDED MONTE CARLO: Neutron Random Walk and Uncertainty in Nuclear Cross Sections, International Conference on Mathematics and Computational Methods applied to Nuclear Science and Engineering (MC 2019)accepted.

[5] F. H. Frohner, Evaluation and analysis of nuclear resonance data, Tech. Rep. 18, IAEA (2000).

[6] N. M. Larson, Updated User's Guide for SAMMY, ORNL, https://info.ornl.gov/sites/publications/files/Pub13056.pdf (October 2008).

[7] D. Brown, M. Chadwick, R. Capote, A. Kahler, A. Trkov, M. Herman, A. Sonzogni, Y. Danon, A. Carlson, M. Dunn, D. Smith, G. Hale, G. Arbanas, R. Arcilla, C. Bates, B. Beck, B. Becker, F. Brown, R. Casperson, J. Conlin, D. Cullen, M.-A. Descalle, R. Firestone, T. Gaines, K. Guber, A. Hawari, J. Holmes, T. Johnson, T. Kawano, B. Kiedrowski, A. Koning, S. Kopecky, L. Leal, J. Lestone, C. Lipitz, J. Márquez Damián, C. Mattoon, E. McCutchan, S. Mughabghab, P. Navratil, D. Neudecker, G. Nobre, G. Noguere, M. Paris, M. Pigni, A. Plompen, B. Pritychenko, V. Pronyaev, D. Roubtsov, D. Rochman, P. Romano, P. Schillebeeckx, S. Simakov, M. Sin, I. Sirakov, B. Sleaford, V. Sobes, E. Soukhovitskii, I. Stetcu, P. Talou, I. Thompson, S. van der Marck, L. Wesler-Sherrill, D. Wiarda, M. White, J. Wormald, R. Wright, M. Zerkle, G. Zeronik, Y. Zhu, ENDF/B-VIII.0: The 8-th Major Release of the Nuclear Reaction Data Library with CIELO-project Cross Sections, New Standards and Thermal Scattering Data, Nuclear Data Sheets 148 (2018) 1–142, https://doi.org/10.1016/j.nds.2018.02.001.

[8] D. Rochman, S. van der Marck, Nuclear data uncertainties for local power densities in the martin-hoogenboom benchmark, Tech. Rep. Joint International Conference of Supercomputing in Nuclear Applications and Monte Carlo, Paris, France, 2013, Nuclear Research and Consultancy Group NGR (2013).

[9] A. Hoefer, O. Buss, M. Hennebach, M. Schmid, D. Porsch, MOCABA: A general Monte Carlo-Bayes procedure for improved predictions of integral functions of nuclear data, Annals of Nuclear Energy 77 (2015) 514–521, https://doi.org/10.1016/j.anucene.2014.11.038.

[10] T. Endo, A. Yamamoto, T. Watanabe, Bias factor method using random sampling technique, Journal of Nuclear Science and Technology 53 (2016) 1494–1501, https://doi.org/10.1080/00223131.2015.1126541.

[11] H. N. Najam, Uncertainty quantification and polynomial chaos techniques in computational fluid dynamics, Annual Revue of Fluid Mechanics 41 (2009) 35–52.

[12] T. Viitanen, J. Leppanen, Explicit treatment of thermal motion in continuous-energy Monte Carlo tracking routines, Nuclear Science and Engineering 171 (2012) 165–173.

[13] C. M. Perfetti, Advanced Monte Carlo Methods for Eigenvalue Sensitivity Coefficient Calculation, PhD Thesis, University of Michigan, 2012.

[14] D. Rochman, A. Koning, al., Nuclear data uncertainty propagation: Perturbation vs. monte carlo, Annals of Nuclear Energy 38 (2011) 942–952.

[15] W. Zwermann, al., Aleatoric and epistemic uncertainties in sampling based nuclear data uncertainty and sensitivity analyses, in: Proceedings of PHYSOR 2012, 2012.

[16] L. L. Carter, E. D. Cashwell, Particle-transport simulation with the monte carlo method, ERDA critical review series TID-26607, https://inis.iaea.org/collection/NCLCollectionStore/$_{P}$*ublic*/07/227/7227109.*pdf*.

[17] I. Lux, L. Koblinger, Monte Carlo Particle Transport Methods: Neutron and Photon Calculations, ECDC Press ISBN 0-8493-6074-9.

[18] T. Viitanen, J. Leppanen, Optimizing the Implementation of the Target Motion Sampling Temperature Treatment Technique - How Fast can it get?, Proceedings of M&C 2013 Sun Valley, ID.

[19] A. de Moivre, The Doctrine of Chance, a method of calculating the probability of events in play, W. Pearson, Second Edition, 1738, https://archive.org/details/doctrineofchance00moiv/page/n5.

[20] P. S. Laplace, Théorie analytique des probabilités, Courier, Imprimeur - Libraire pour les Mathématiques et la Marine, 1812, https://archive.org/details/thorieanalytiqu01laplgoog/page/n7.

[21] R. N. Hwang, A rigorous pole representation of multilevel cross sections and its practical applications, Nucl. Sci. Eng. 96 (1987) 192–209.

[22] R. N. Hwang, An Extension of the Rigorous Pole Representation of Cross Sections for Reactor Applications, Nucl. Sci. Eng. 111 (2) (1992) 113–131.

[23] R. N. Hwang, Recent developments pertinent to processing of endf/b-6 type resonnance cross section data, International Conference on the Physics of Nuclear Science and Technology.

[24] B. Forget, S. Xu, K. Smith, Direct doppler broadening in monte carlo simulations using the multipole representation, Annals of Nuclear Energy 64 (2014) 78–85.

[25] C. Josey, P. Ducru, B. Forget, K. Smith, Windowed multipole for cross section doppler broadening, Journal of Computational Physics 307 (2016) 715–727.

[26] J. Liang, P. Ducru, B. Forget, Target Velocity Sampling for Resonance Elastic Scattering using Windowed Multipole Cross Section Data, Transactions of the American Nuclear Society 119 (2018) 1163–1166, http://dx.doi.org/10.1016/j.jcp.2017.01.039.

[27] P. Ducru, G. Hale, M. Paris, V. Sobes, B. Forget, Scattering matrix pole expansions & invariance with respect to R-matrix parameters, arXivhttps://arxiv.org/abs/1903.02661.

[28] P. Ducru, V. Sobes, G. Hale, M. Paris, B. Forget, Windowed multipole representation of R-matrix cross sections, Physical Review C 00 (0) (2019) 000–000, work-in-progress.

[29] F. Brown, B. Kiedrowski, Continuous-energy sensitivity coefficient capability in mcnp6, American Nuclear Society Winter Meeting.

[30] D. E. Cullen, Exact doppler broadening of tabulated cross sections, Nuclear Science and Engineering 60 (1976) 199–229.

[31] P. K. Romano, N. E. Horelik, B. R. Herman, A. G. Nelson, B. Forget, K. Smith, OpenMC: A state-of-the-art Monte Carlo code for research and development, Annals of Nuclear Energy 82 (2015) 90 – 97, joint International Conference on Supercomputing in Nuclear Applications and Monte Carlo 2013, SNA + MC 2013. Pluri- and Trans-disciplinarity, Towards New Modeling and Numerical Simulation Paradigms. doi:https://doi.org/10.1016/j.anucene.2014.07.048.
URL http://www.sciencedirect.com/science/article/pii/S030645491400379X

[32] B. Gustavsen, Improving the pole relocating properties of vector fitting, IEEE Transactions on Power Delivery 21 (3) (2006) 1587–1592, DOI: 10.1109/TPWRD.2005.860281.

[33] G. Arbanas, V. Sobes, A. Holcomb, P. Ducru, M. Pigni, D. Wiarda, Generalized Reich-Moore R-matrix approximation, EPJ Web of Conferences 146 (12006), https://doi.org/10.1051/epjconf/201714612006.

[34] P. Ducru, V. Sobes, B. Forget, K. Smith, On methods for conversion of R-matrix resonance parameters to multi-pole formalism, in: Proceedings of PHYSOR 2016, 2016, pp. 2138–2150.